



Modelling debris-covered glacier dynamics: transient response to changes and feedbacks in debris and climate forcing

Florian Hardmeier¹, James C. Ferguson^{1,2}, and Andreas Vieli¹

¹Department of Geography, University of Zurich, Switzerland

²Institute of Science and Technology Austria, Klosterneuburg, Austria

Correspondence: Florian Hardmeier (florian.hardmeier@geo.uzh.ch)

Abstract. Glaciers worldwide are becoming increasingly debris-covered, yet many parts within the coupled glacier-debris system are not well-understood. While the insulating effect of debris is well-known, observations of debris cover are scarce, often limited by logistical challenges. The main aim of the study is to better understand the complex transient glacier response and debris-induced feedbacks through numerical flow modelling. We present a newly developed 1-dimensional flowline model that couples ice flow, depth-resolved debris transport, and debris cover impact on mass balance. This approach allows for a detailed examination of the dynamics of debris-covered glaciers under transient forcing conditions of climate and debris input over extended timescales. Our results indicate that low-amplitude, decade-scale variability in debris or climate forcing does not significantly impact glacier evolution. However, large debris supply events can have a sustained impact. We find that debris-covered glacier response to warming climate forcing is non-monotonic, with distinct phases of thinning, retreat, and long-term re-advance. We attribute this to a separate, longer timescale process of englacial debris transportation. Additionally, feedbacks in the englacial debris trajectory and complex bed topography further increase the non-linearity of transient glacier response.

1 Introduction

Debris-covered glaciers are found in all glaciated mountain ranges and are particularly common in high relief mountain areas. In recent years, there has been growing interest in debris-covered glaciers, as under the current warming, the number of debris-covered glaciers and their percentage of debris-covered area is substantially increasing (Anderson, 2000; Kirkbride and Deline, 2013). Yet we do not fully understand many elements and interactions of the debris-covered glacier system in a changing climate.

Debris cover is, above a thickness of a few centimeters, known to protect the ice from surface ablation (Østrem, 1959; Mattson et al., 1993; Nicholson and Benn, 2006) and thereby changes the spatial patterns of surface mass balance compared to those on debris-free 'clean-ice' glaciers (Nicholson and Benn, 2006). The accumulated debris on the surface therefore reduces the ablation there and leads to today's typically observed, extended debris-covered glacier tongues (Benn et al., 2012; Kirkbride and Deline, 2013; Carturan et al., 2013). Considering debris thickness and its insulating effect statically is, however, not sufficient for understanding the evolution of debris-covered glaciers, as the debris is being transported along and within the glacier and hence its thickness is strongly linked to ice dynamics. A more dynamically active glacier may for example lead to



25 thinner debris thicknesses as the debris has less time to accumulate on the surface (Anderson et al., 2021). Furthermore, debris thickness also depends on the rate and location of debris input to the glacier. Debris deposited in the accumulation area is entrained into the ice and is first transported englacially before it melts out in the ablation area and impacts on surface ablation.

Interestingly, thinning and related mass loss from debris-covered glaciers is often observed to occur at rates similar to those on clean-ice glaciers (Pellicciotti et al., 2015; Salerno et al., 2017). This has been explained on the one hand by the occurrence 30 of melt-enhancing features such as ice cliffs and supraglacial ponds (Kneib et al., 2023) and on the other hand by a reduction in dynamic ice replacement (Banerjee, 2017; Anderson et al., 2021), which both are related to dynamic stagnation. This highlights again the importance and complexity of dynamic feedbacks between debris related processes and ice flow dynamics for understanding the evolution of debris-covered glaciers.

Debris is usually deposited on the glacier surface by gravitational processes, where it is entrained in the ice (accumulation area) 35 or transported along on the surface (ablation area). The stochastic nature of the debris supply processes such as avalanches and rockfalls, as well as the challenges in accessibility, makes them difficult to observe and quantify (Heimsath and McGlynn, 2008; Scherler and Egholm, 2020). Current approaches of estimating debris supply rates therefore often rely on assumed headwall 40 erosion rates or indirect inferences from debris fluxes on the glacier tongues (Heimsath and McGlynn, 2008; Banerjee and Wani, 2018; McCarthy et al., 2022). The latter generally rely on steady-state assumptions and the impact of temporal variations of debris supply rates on debris thicknesses and hence glacier evolution remains largely unknown.

As debris is transported along either englacially or supraglacially, understanding the transport paths and interaction with flow dynamics is essential for improving our understanding of the entire system. Due to the reduced ablation on debris-covered 45 tongues, dynamic adjustments in glacier length are expected to be slower, on a century rather than a decadal timescale, and hence mostly beyond the observational record (Ferguson and Vieli, 2021). Also, given the current warming trend, today's observations are almost exclusively limited to the dynamic states of retreat and stagnation and therefore contain some inherent 50 but unknown bias (Ferguson and Vieli, 2021).

To better understand the evolution and dynamic feedbacks in the debris-covered glacier system, it is therefore crucial to dynamically couple the involved processes from debris input, transport, glacier flow, debris thickness evolution, and its effect 55 on surface mass balance. Further, we need to consider the transient response of the debris-covered glacier system to a variable climate and debris input, beyond the observational record. Numerical flow modelling allows for quantitatively coupling and evolving ice flow, glacier and debris evolution. A limited number of dynamic modelling studies have attempted to do this. However, they vary strongly in the way they include the effects of debris and its interaction with glacier flow, depending on the research questions to be addressed and the related simplifications made.

There are three main approaches of treating debris in transient glacier flow models. The first set of models prescribe the 55 spatial debris thickness patterns on the surface in order to account for their reduction on ablation without explicitly considering debris transport. The simplest approach assumes a spatially fixed and uniform debris thickness in a flowline model (e.g. Banerjee and Shankar (2013)) to capture the effect of debris on mass balance in isolation and to investigate the effect of dynamic stagnation on thinning rates. The horizontally distributed model by Compagno et al. (2022) uses empirically derived spatial



thickness patterns based on mapping from satellite data and evolves its extent and thickness in relation to the equilibrium line
60 altitude (ELA). This approach was used to assess the effect of debris cover on future mass loss of High Mountain Asia.

A second set of models includes, in addition to the effect of debris on ablation, the linking of supraglacial debris flux to surface velocity. The most basic such models focus on the case where debris is deposited solely on the glacier surface in the ablation area (Vacco et al., 2010; Verhaegen et al., 2020). More advanced versions also consider a simple approach of debris input in the accumulation area by prescribing a uniform debris concentration within the ice (Vacco, 2009; Ferguson and Vieli, 65 2021; Mayer and Licciulli, 2021). In the ablation area this debris melts out at the surface and is added as a source term to the debris layer thickness evolution. This approach still avoids having to explicitly model debris transport within the ice. It has, however, the disadvantage that debris concentration is constant in space and if varied over time its effect is immediate everywhere, as any transport delay from the deposition area to the melt-out position is ignored. Furthermore, thinning or thickening of englacial debris bands due to ice flow can not be considered. These models were mostly used on synthetic simple 70 glacier geometries to assess simple climate change experiments such as delayed length responses, typical thinning patterns and effects of melt enhancement features, for example from debris free ice cliffs (Ferguson and Vieli, 2021; Mayer and Licciulli, 2021).

The third set of models includes an explicit treatment of englacial debris by transporting the debris through the glacier using either an Eulerian approach, advecting debris concentration on a grid (Rowan et al., 2015; Anderson and Anderson, 75 2016; Wirbel et al., 2018; Rowan et al., 2021; Ferguson, 2022), or by tracking debris as Lagrangian particles (e.g. in the integrated second-order Shallow Ice Approximation model iSOSIA: Egholm et al. (2011); Margriner et al. (2025)). The latter approach has so far solely focused on the investigation of 3-dimensional debris particle pathways for given deposition rates (Egholm et al., 2011). For the former approach, Anderson and Anderson (2016) were the first to combine a full englacial and supraglacial debris advection scheme with a debris-coupled mass balance and localized debris input area. This approach 80 has so far largely been used to explore the effect of debris deposition locations and steady debris input rates or climates on glacier extents (Anderson and Anderson, 2016) and to better understand thinning patterns from glaciers in a warming climate (Anderson et al., 2021). The time-transient aspect of debris input and the interaction with fluctuating climates have, however, not been systematically investigated, as most approaches have not explicitly separated surface accumulation from debris input rates.

85 The main novelties of this study are the examination of both temporally variable debris input and transient climate forcing to debris-covered glaciers and an in-depth analysis of the involved feedbacks, and response times from the related englacial debris transport. We present a new numerical flow model that couples ice and debris dynamics to examine the combined effects and feedbacks in the debris-covered glacier system. Our approach unites many elements from other studies, using a flowline model with depth-resolved (2D) Eulerian debris transport as in Anderson and Anderson (2016). Our novel debris entrainment 90 implementation allows us to independently control climate and debris forcing to explore the transient feedbacks between them. Our approach further enables the separation of detached ice masses, which is becoming increasingly common for glaciers with complex bed topography (Pellicciotti et al., 2015; Rippin et al., 2020; Rowan et al., 2021). To examine the validity of our model, we perform benchmark experiments as conducted in previous approaches (Anderson and Anderson, 2016; Ferguson



and Vieli, 2021; Ferguson, 2022). We explore fundamental relationships that govern the geometry of debris-covered glaciers, 95 depending on debris supply, ELA, and topography. We investigate the non-linear dynamic response to warming that is specific to debris-covered glaciers. One main focus lies on the role of englacial debris transport in producing unique and previously unexplored long-term feedbacks in this response. For this purpose, we conduct a series of experiments, forcing the model with increasing complexity. We start with a steady climate, then introduce step-change perturbations and periodic fluctuations, and finally approach a realistic Alpine climate (Lüthi, 2014; Masson-Delmotte et al., 2021).

100 We conduct additional experiments to determine the timescales and magnitudes to which debris-covered glaciers are sensitive to in terms of climate and debris input variations. We quantify long-term glacier response times that are relevant for predicting the future state of debris-covered glaciers and the timing of their retreat. We also take an in-depth look at deficits and surpluses of debris flux within a transient system, potentially informing future studies relying on debris flux as a metric of debris transport, supply and export.

105 2 Methods

We use a Shallow Ice Approximation (SIA) based flowline model that we adapted from Ferguson (2022), which is similar to the approach used in Anderson and Anderson (2016). The model is capable of tracking englacial and supraglacial debris transport by advecting debris concentrations. Compared to previous approaches that use a uniform debris concentration (e.g. Rowan et al. 110 (2015); Ferguson and Vieli (2021)), we aim here at more realistic modelling of glacier debris interaction that allows us to model temporally and spatially variable debris input and transient climates. Building on the modelling approach by Anderson and Anderson (2016) we track the englacial debris by advecting the debris concentration as a Eulerian variable on a 2-dimensional grid. Our approach differs mainly in the way we treat debris entrainment in the accumulation area and debris removal at the glacier terminus. We further advance the original model by Ferguson (2022) by more explicitly separating forcings in debris input and climate as well as investigating model sensitivities and robustness in performance in detail (Appendix B).

115 2.1 Ice dynamics

The evolution of a glacier is fundamentally forced by the surplus of ice mass in the accumulation area and the removal in the ablation area, resulting in a viscous flow down the slope. The constitutive equation of ice flow is non-linear and solving the full equations is computationally expensive. We therefore use the simplified approach of the Shallow Ice Approximation (SIA), first developed by Fowler and Larson (1978). With our focus on the along-flow glacier evolution and debris transport, and to 120 further reduce computational costs, we use a flowline version of the SIA which computes ice flux from the local ice thickness and along flow surface slope. Following (Ferguson, 2022), when assuming SIA ice flow, the equations for the evolution in ice thickness $H(x, t)$ of a glacier flowing along the down-glacier direction x with depth-averaged velocity $\bar{u}(x, t)$ and in response to a surface mass balance forcing $a(x, t)$ are given by:

$$\frac{\partial H}{\partial t} + \frac{\partial(\bar{u}H)}{\partial x} = a, \quad (1)$$



125
$$\bar{u} = \frac{2A(\rho g)^n}{n+2} H^{n+1} \left| \frac{\partial h}{\partial x} \right|^{n-1} \frac{\partial h}{\partial x}, \quad (2)$$

where ρ is the density of ice, g the gravitational acceleration, A and n are the rate factor and exponent from Glen's flow law, respectively, and $h(x, t) = H + b$ is the glacier surface elevation for a given bed elevation $b(x)$. The evolution equation for ice thickness (Eq. 1) is solved on a regular horizontal grid with grid size dx .

130 In order to track the debris within the glacier (Sect. 2.2), we have to additionally resolve the depth-dependent velocity field $\mathbf{u} = (u(x, \hat{z}, t), w(x, \hat{z}, t))$, where w is the vertical velocity and $\hat{z} = (z - b)/H$ is the fractional height (0 = bed, 1 = surface) within the ice column. Then the depth dependent velocities are given by

$$u(\hat{z}) = \frac{n+2}{n+1} \bar{u} (1 - \hat{z}^{n+1}) \quad (3)$$

135
$$w(\hat{z}) = -\frac{\partial \bar{u}}{\partial x} \left[1 - \hat{z} \left(\frac{n+2}{n+1} - \frac{\hat{z}^{n+1}}{n+1} \right) \right]. \quad (4)$$

2.2 Debris dynamics

Using this depth-dependent velocity field we can now track the englacial debris concentration C as it is advected passively through the glacier according to

$$\frac{\partial C}{\partial t} + \nabla \cdot (\mathbf{u}C) = \psi, \quad (5)$$

140 where $\psi(x, t)$ is a debris forcing (input) function defined at the surface (Sect. 2.4). A logical way to solve this problem numerically is to work in coordinates of (x, \hat{z}) so that the glacier domain is effectively rectangular with the bed at $\hat{z} = 0$ and the surface at $\hat{z} = 1$. Correcting for the thinning or thickening of the glacier with time as well as the spatial gradient in ice thickness along the direction of flow results in an equation for debris concentration evolution given by Anderson and Anderson (2016):

145
$$\frac{\partial C}{\partial t} + \nabla \cdot (\mathbf{u}C) + \frac{C}{H} \frac{\partial H}{\partial t} + \frac{uC}{H} \frac{\partial H}{\partial x} = \psi. \quad (6)$$

Once debris reaches the surface, it melts out at a rate given by the debris concentration $C_s(x, t)$ at the surface and the ablation rate. The debris thickness evolves according to:

$$\frac{\partial D}{\partial t} + \frac{\partial (u_s D)}{\partial x} = -C_s a, \quad (7)$$



where u_s is the surface velocity and D is the debris cover thickness. We quantify debris transport as an along-glacier flux,
 150 where debris flux Q_d is the sum of supraglacial and englacial debris flux, defined as

$$Q_d = u_s D + \int_0^1 u(\hat{z}) C(\hat{z}) h_{\hat{z}}. \quad (8)$$

For the glacier to remain in balance, it maintains a constant debris flux Q_d (Fig. B5) throughout its length, building an increasingly thick debris layer where velocities decrease. During phases of retreat, lowered ice velocities lead to temporarily decreased Q_d , while advance leads to a temporary debris flux surplus.

155 **2.3 Surface mass balance**

We assume the debris-free surface mass balance $\tilde{a}(z)$ to be linearly dependent on elevation:

$$\tilde{a}(z) = \min\{\gamma(H + b - \text{ELA}), a_{max}\}, \quad (9)$$

where γ is the mass balance gradient, ELA is the equilibrium line altitude, and a_{max} is a maximum mass balance, which limits the accumulation at high elevations. The mass balance rate a for debris-covered surfaces then includes the well-established
 160 melt-reducing effect of surface debris on surface ablation that is inversely proportional to debris thickness D and results in

$$a = \tilde{a} \frac{D_0}{D_0 + D}, \quad (10)$$

where D_0 is the characteristic debris thickness, describing the shape of the Østrem curve. The value we use for D_0 (0.065 m) is the default value from Anderson and Anderson (2016). Literature values of D_0 vary strongly, previous analysis (Hardmeier, 2022) shows that substantially higher values (e.g. 0.15 m) have been inferred from observations (Fig. C2).

165 To quantify the glacier-wide reduction in ablation caused by debris cover we establish an ELA compensation term 'dELA'. For a given constant debris supply, dELA is the difference between debris-free and debris-covered (steady-state) ELA that is required to force a glacier of equivalent length or volume. To calculate dELA, we very slowly and linearly increase the ELA (by steps of 0.1 m yr^{-1}) for a debris-free and a variety of debris-covered glaciers with different input rates. For each ELA, we assign the modelled volume and length, allowing us to compare the ELAs that correspond to the same volume or length. dELA
 170 essentially describes the amount of warming that can be directly compensated by debris cover, either measured by length or volume. This enables us to analyze the direct relationship between the glacier system and debris supply (Sect. 3.1.2) in simple terms.

2.4 Debris entrainment and melt-out at the surface

Next, we describe the supply of debris onto the glacier surface and how it is entrained into the ice in case of the accumulation
 175 area. In contrast to Ferguson (2022) we do not prescribe a debris concentration in the surface layer but rather control the debris



supply rate itself along the glacier surface. Debris supply is thereby independent of climatic forcing and when combined with the accumulation rate then defines the debris concentration at the surface boundary.

In the uppermost layer of our existing along-flow profile grid, C_s , we compute the surface debris concentration by integrating 180 the prescribed debris input rate d_{in} . As opposed to Ferguson (2022), we want to control exactly how much debris enters the system in a given debris input area and keep it independent of climate or more specifically of the ice accumulation rate. Finally, we also want to allow debris deposition in the ablation area.

We distinguish two cases in our implementation of debris input: case A, where the debris input occurs in the accumulation 185 area ($a(x, t) > 0$), and case B, where debris input occurs in the ablation area ($a(x, t) \leq 0$). In case A (Fig. 1a), debris is entrained into the ice through integrating the concentration C_a of the accumulated surface layer into the uppermost grid cell. At time step t , the concentration in the surface grid cell with vertical size h_z is then a result from three components: the existing concentration in the cell from the previous time-step $C_s(t-1, j)$, the advected concentration from the upstream cell $C_s(t-1, j-1)$ (gray in Fig. 1a), and the forcing layer concentration C_a from debris deposition, which results in:

$$190 \quad C_s(t) = \frac{w}{h_z} C_a + (1 - \frac{w}{h_z})(1 - u) * C_s(t-1) + (1 - \frac{w}{h_z})u * C_s(t-1, j-1), \quad (11)$$

with $C_a = d_{in}/a$,

where d_{in} is a user-defined absolute debris input rate. This means that changes in both the debris input rate as well as the ice accumulation rate will affect the input debris concentration in the surface grid cell. In case B (ablation area), debris does not enter into the ice and is instead added directly to the surface debris layer with thickness D at the rate d_{in} .

195 Debris melt-out d_{out} in the ablation area, a sink for debris concentration at the boundary of the englacial grid and a source for the debris thickness D , is given by:

$$d_{out} = C_s a / h_z. \quad (12)$$

2.5 Terminal debris boundary condition

At the terminus, we follow Ferguson and Vieli (2021) and assume the surface debris to slide off the glacier at a terminal ice 200 cliff of a critical height H^* , as expressed in Equation 13 below. When ice thickness falls below this critical value, surface mass balance a is set equal to the debris-free mass balance \tilde{a} over the fraction of the grid cell that is covered by the ice cliff. This approach avoids an infinite piling up of debris near the terminus where horizontal ice flow goes to zero in the SIA-approximation. It is supported by the observation of terminal ice cliffs typical at debris-covered glacier termini, in particular for currently retreating glaciers (Ferguson and Vieli, 2021).



Case A: Mass balance > 0

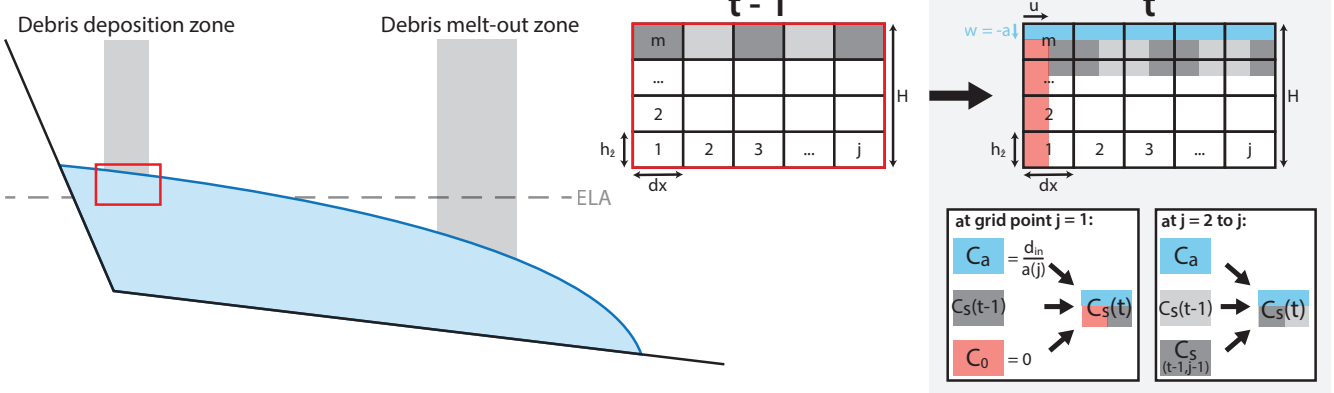


Figure 1. Implementation of debris entering the 2-dimensional grid as a concentration in the user-defined input area if in the accumulation area (mass balance > 0). The evolution of C_s , the debris concentration in the uppermost cell, at grid point j between time steps $t - 1$ and t is defined in Equation 11. C_a is the debris concentration in newly accumulated ice, computed from debris input rate d_{in} and surface mass balance a . C_0 is concentration in the debris-free layer advected along ice velocity u from upstream of the debris input area.

$$205 \quad a = \begin{cases} \tilde{a} \frac{D_0}{D_0 + D}, & \text{where } H > H^* \\ \tilde{a}, & \text{where } H \leq H^* \end{cases} \quad (13)$$

2.6 Numerical implementation

The basic numerical implementation of this model is described extensively in Ferguson and Vieli (2021) and complemented for the englacial tracking part in Ferguson (2022). In summary, the debris–ice system is resolved through the application of finite differences. The surface evolution of ice flow is discretized using forward differences and discretizations, whereas 210 debris transport uses centered differences both on regular horizontal ($dx = 50$ m) and vertical ($m = 40$ layers) grids. To ensure numerical stability we ensure to satisfy the Courant-Friedrich-Levy (CFL) condition (Courant et al., 1928). Special attention is also given to numerical diffusion in englacial debris transport, which is counteracted by implementing an anti-diffusion advection scheme in Smolarkiewicz (1983). Debris input and melt-out are computed through the boundary condition in the uppermost layer of the grid (Eq. 11 and 12).

215 2.7 Experimental setup

We use a simple synthetic bed geometry similar to Ferguson and Vieli (2021) that represents a typical debris-covered glacier and is constant and gently sloped at 5.7 degrees (or 100 m of elevation per km distance) for the main trunk of the glacier and has a steep (45 degrees) headwall above (e.g. Fig. 2). The ELAs are generally chosen to be well below the headwall and with debris



input in the accumulation area (but still below the headwall) as we are mainly interested in the case of englacial debris transport.

220

In general, we first create a debris-covered glacier for a standard reference parameter set (Table 1), by building up a clean-ice glacier for a given ELA, then adding the debris in the debris input area and running it to a steady state. If not stated differently this glacier geometry will then serve as the initial state for further experiments.

225

We then perform a suite of modelling experiments, where we first consider steady-states (Sect. 3.1), mostly adapting and re-evaluating experiments conducted in previous studies (Anderson and Anderson, 2016, 2018; Ferguson, 2022). We then explore transient responses (from Sect. 3.2) to variable climates (labeled as clim- x experiments) and debris inputs (labeled as deb- x ; see Table 2). The considered time spans are usually 3000 or 6000 years, which is rather long but necessary due to the expected slow adjustment timescales of debris-covered glaciers (Ferguson and Vieli, 2021). These experiments are conducted 230 using the parameters provided in Table 1. An overview of all experiments and respective forcing variable ranges is given in Table 2. The parameter ranges are mostly extracted from the modelling literature (e.g. Anderson and Anderson (2016); Ferguson (2022)). To further test and better understand the robustness of the model we undertook additional sensitivity and validation experiments related to model reversibility, debris mass conversation, characteristic debris thickness D_0 , ice rheology and terminal ice cliff height. These results are presented in detail in Appendices B & C, but integrated in the discussion 235 on the main model experiments where relevant. For consistency across all experiments we define a reference model parameter set (Table 1) and vary only forcing variables, while other parameters are considered fixed and only explored in Appendix C.

3 Modelling experiments and results

240

In this section we perform our main modelling experiments with a particular focus on the transient response of debris-covered glaciers to changes in debris input and climate. The experiments are structured along an order of increasing forcing complexity, where we first consider steady-states (Sect. 3.1) before moving on to simple transient responses (from Sect. 3.2), and finally exploring more realistic model forcing in Sect. 3.4.

3.1 Steady-states

245

In a first step, we explore various sets of constant forcing variables and their corresponding steady-state glacier geometries. From these stable states we assess the impact of the inclusion of debris cover on the glacier geometry and debris thickness distribution in an otherwise constant set of forcing variables and parameters.



Table 1. Forcing variable ranges and reference model parameters for the numerical experiments.

Forcing variables	Name	Value in reference experiment	Units
ELA	Equilibrium line altitude	2900	m
d_{in}	Debris input rate	0.0045	m yr^{-1}
L_d	Debris input area length	400	m
x_d	Debris input area position*	0	m

Fixed parameters	Name	Value	Units
ρ	Density of ice	910	kg m^{-3}
g	Gravitational acceleration	9.81	m s^{-2}
A	Flow law parameter	2.4×10^{-24}	$\text{Pa}^{-3} \text{ s}^{-1}$
n	Glen's constant	3	
D_0	Characteristic debris thickness	0.065	m
a_{max}	Maximum surface mass balance	2	m yr^{-1}
γ	Surface mass balance gradient	0.0075	yr^{-1}
H^*	Terminal ice thickness threshold	30	m
dt	Time step	0.005	yr
dx	Horizontal discretization	50	m
m	Number of vertical grid cells	40	
θ	Bed slope	0.1	m m^{-1}
θ_c	Headwall slope	1	m m^{-1}

*relative to headwall slope break

3.1.1 Effect of debris supply rate and location on glacier geometry

To assess the relationship between a glacier and debris cover, we first compare steady-states of a debris-free glacier to the case 250 where we add debris at a fixed rate and fixed location below the headwall (but above the ELA). We observe that the general shapes in surface geometry of the debris-covered glacier compared to the debris-free one is largely congruent (Fig. 2a). Only below the position where debris starts to emerge the two surfaces start to diverge (at around 6 kilometers). The debris-covered glacier produces a more elongated tongue sustained through the insulating effect of the debris. The along-glacier shape of the debris thickness is slightly convex-up in the melt-out area, transitioning to a concave-up shape near the terminus (Fig. 2b), as 255 previously observed by Anderson and Anderson (2018). Note that the flattening of the surface in the debris melt out area can also be seen in the slight decrease in velocity there (between 4 and 7 km along the glacier).

When forcing the model with different, but still time-constant debris input rates (Fig. 3), the glacier surface profiles are still



Table 2. Overview of undertaken numerical experiments.

ID	Name	Variable	Details	Figure(s)
<i>Steady-state</i>				
steady-1	Clean-ice vs. debris-covered	d_{in}	0 or 4.5 mm yr ⁻¹	Fig. 2
steady-2	Variable d_{in} steady-states	d_{in}	1.0–22.5 mm yr ⁻¹	Fig. 3 & 5
steady-3	Variable debris input area	x_d	0, 800, 4000 m	Fig. 4
<i>Variable climate</i>				
clim-1	ELA step-change	ELA	2900–3000 m	Fig. 6 & 7
clim-2	Slow ELA increase	ELA	0.1 m yr ⁻¹ increase	Fig. 5
clim-3	Sine ELA	ELA	2950–3050 m; $\lambda = 100$ –500 yr	Fig. 9
clim-4	Complex ELA	ELA	Climate history & scenarios	Fig. 10 & 11
clim-5a	Complex bed & steady-state ELAs	ELA	2600–2800 m	Fig. 12
clim-5b	Complex bed & complex ELA	ELA	Climate history & scenarios	Fig. 13
<i>Variable debris</i>				
deb-1	d_{in} step-change	d_{in}	0–22.5 mm yr ⁻¹ ; duration = 1–2000 yr	Fig. 7, B1
deb-2	Sine d_{in}	d_{in}	1–8 mm yr ⁻¹ ; $\lambda = 100$ –500 yr	Fig. 9
deb-3	d_{in} spike	d_{in}	1 m yr ⁻¹ for 1 yr	Fig. 8 & B2

very similar but substantially more elongated with increasing debris input rate d_{in} (Anderson and Anderson, 2016). Total
 260 surface debris volume (Fig. 3c) thereby scales non-linearly with increasing d_{in} , as both local debris cover thickness and the
 covered glacier length increase. The mass balance gradient (Fig. 3b) starts to be reversed in the upper debris-covered area with
 increasing debris input, but stabilizes relatively quickly further below as the increasing, elevation-dependent clean-ice ablation
 is compensated by insulation from debris thickening.

265 In a next step, we assess the impact of the debris deposition location by comparing two accumulation area cases (Fig. 4),
 one closer to the headwall than the other, and one ablation area case, set up similarly by Anderson and Anderson (2016). We
 observe that when moving debris input closer to the ELA, the englacial transport trajectory gets shorter and the debris melt-out
 area moves up-glacier, with the glacier ultimately increasing in length. The ablation area case, with the debris input closest
 270 to the ELA, leads to the largest debris-covered area (Fig. 4c) and consequently to the most elongated glacier, as ablation is
 reduced already further up-glacier and therefore over a larger part of the ablation area (Fig. 4b), which is in line with the earlier
 modelling by Anderson and Anderson (2016). In general, the impact on steady-state glacier length from changing debris input
 locations remains in our case relatively small (below a few percent) and the maximum debris thickness at the terminus is rather
 similar for all cases with our reference parameter set. As Anderson and Anderson (2016) describe, the impact of debris input
 location increases with increasing input rate.

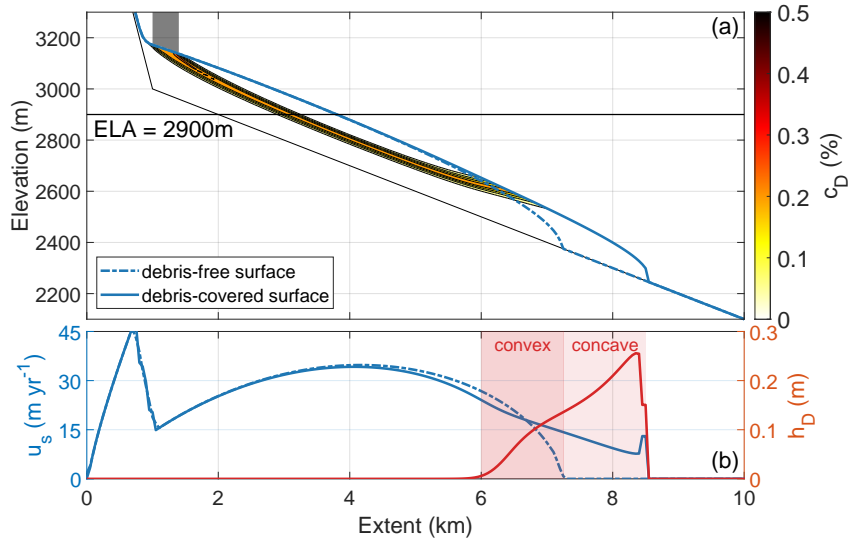


Figure 2. Experiment steady-1: (a) steady-state surface geometries for a debris-free and a debris-covered glacier with the same constant ELA at 2900 m (blue lines). For the debris-covered glacier, the gray area marks the 400 m wide debris input area with input rates of 4.5 mm a^{-1} , the colored areas within the glacier indicating the englacial debris concentrations in %. (b) Surface velocities of the debris-covered and debris-free glaciers (blue) and corresponding debris thickness h_D (red), where the light red areas mark convex-up and concave-up sections of the along-flow debris cover distribution.

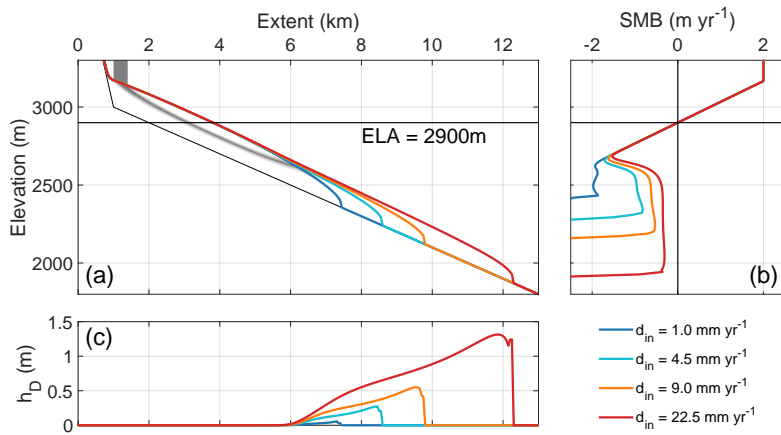


Figure 3. Experiment steady-2: Steady-state glaciers for variable debris input rates d_{in} ($1.0, 4.5, 9.0$, and 22.5 mm yr^{-1}) with otherwise the same parameter setting as in Fig. 2 with the resulting steady-state (a) glacier surface geometries, (b) surface mass balance, and (c) debris cover thickness h_D . The gray area marks the debris input area below the headwall and the englacial debris transport trajectory.

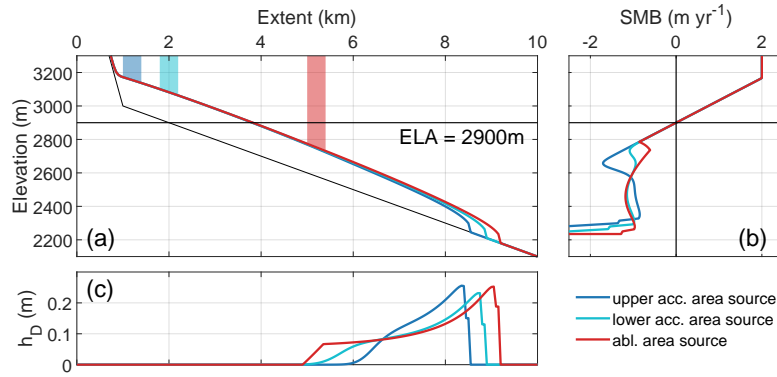


Figure 4. Experiment steady-3: Steady-state glaciers for different debris input area locations (0, 800, and 4000 meters from headwall slope break) using the same debris input rate of 4.5 mm a^{-1} and an ELA of 2900m with the resulting steady-state glacier (a) surface geometries, (b) surface mass balance, and (c) debris cover thickness h_D .

275 3.1.2 Compensation of warming-induced melt by debris cover

Here, we directly put the ablation reduction effect of debris cover into perspective by comparing it to a (permanent) change in ELA, comparing debris-free and debris-covered glaciers by finding the ELAs where their size is equivalent. The concept of dELA (as established in Sect. 2.3) describes this comparison, relating steady-state debris-free ELA to a corresponding debris-covered ELA that both lead to a glacier equivalent in either volume or extent. Figure 5 shows this comparison for four 280 debris-covered glaciers with different debris input rates d_{in} ($1.0 - 22.5 \text{ mm yr}^{-1}$). Both volume- and extent-derived dELA show a linear relationship to d_{in} (Fig. 5a). We can infer from this that steady-state glacier size linearly scales with debris input, as is also apparent from Figure 3a. The thin, elongated shape of debris-covered termini mean that dELA of extent is consistently about double that of the volume, meaning that an increase in debris input would affect glacier length much more strongly than ice volume. As equivalent debris-covered ELAs (colored lines in Fig. 5b) run parallel to debris-free ELA (black line), dELA, 285 which is former subtracted by the latter, remains mostly constant (independent of elevation) as long as the ELA is not in the vicinity of the headwall (around 3100 to 3200m). To summarize, debris-induced glacier elongation is linearly dependent on debris input and independent of ELA.

3.2 Transient response to step-change forcing

Next, we apply simple transient forcings to the model and investigate the dynamic glacier response starting from the reference 290 setup (Table 1). In a first set of experiments we apply an abrupt change in ELA (experiment clim-1) or debris forcing (experiment deb-1), which we name as 'step-change' in forcing. Over the long timescales of glacial response in experiments, an abrupt change in climate temperature as modelled here is quite similar to concurrent sub-century scale climate change. Still, climate conditions on real glaciers are subject to perpetual variations, never truly allowing a 'steady-state'. This is why we later move

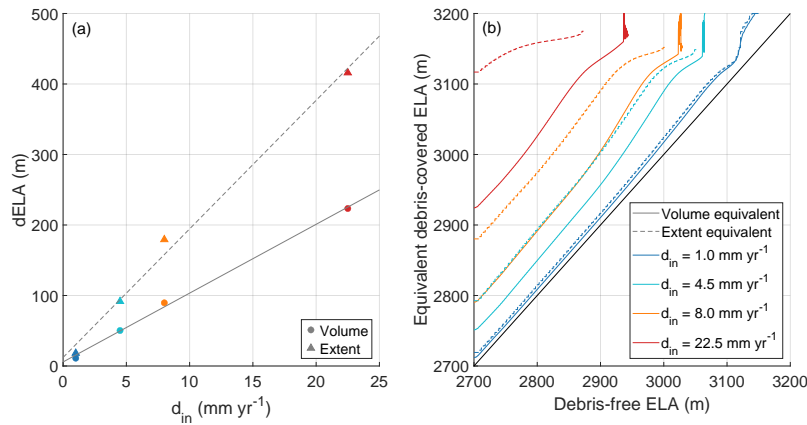


Figure 5. Experiments steady-2 & clim-2: (a) Relationship of steady-state debris input with dELA (dELA = equivalent debris-covered ELA – debris-free ELA, measured at 2700 m debris-free ELA) for volume and extent equivalent ELAs, showing a roughly linear relationship. (b) Debris-free ELA compared to debris-covered ELA, showing the debris-covered ELA required to result in a volume or extent equivalent to the debris-free case. Four cases are shown, with a debris input of 1.0 mm yr^{-1} (blue), 4.5 mm yr^{-1} (cyan), 8.0 mm yr^{-1} (orange), and 22.5 mm yr^{-1} (red).

on to periodic variation experiments (clim-3 & deb-2 in Sect. 3.3) and more stochastic (deb-3) and realistic (clim-4 & clim-5) variations (in Sect. 3.4).

3.2.1 Step-change in ELA

Figure 6 shows the response to a step-change warming (a & c) and cooling (b & d: experiments clim-1) by a change in ELA of 100 meters, in order to investigate differences in dynamic response between debris-covered and debris-free glaciers. In the advance experiment (ELA lowering; Fig. 6b & d), the length response of the debris-covered glacier is almost indistinguishable 300 from the debris-free glacier response as demonstrated by the almost identical shape of the advance curves. The advance is accompanied by an initial decrease in total surface debris (Phase 4 in Fig. 6d/f) as the debris melt-out position moves down-glacier. Once this melt-out position is stabilized, surface debris increases (Phase 5) as the debris-covered tongue advances (Video Supplement 1).

305 In the retreat case (Fig. 6a & c; increased ELA), the response of the debris-covered glacier, however, distinctly differs from the debris-free case. In a first phase (Phase 1 in Fig. 6c/e), the debris-free glacier starts retreating almost immediately as a result of increased mass loss and thinning (Fig. 6c), whereas the debris-covered glacier terminus remains and does not retreat for several decades, despite already rapidly losing mass. In Phase 1, it already starts accumulating more debris at the surface (Fig. 6e), due to enhanced debris melt-out and an expanding surface debris area (see increase of total debris by red line). In a second 310 phase lasting a few decades (Phase 2), the debris-covered glacier abruptly retreats as the glacier tongue eventually thins away



and collapses (blue solid line in Fig. 6c) and the terminal section with thick debris cover is now removed, hence the remaining total debris volume on the glacier surface strongly reduces (black line in Fig. 6e). In a third phase that lasts centuries (Phase 3), the glacier recovers slowly from its maximal retreated length position to a slightly more advanced new stable retreated state (Fig. 6c). During Phase 3, the supraglacial debris volume slowly builds up again to reach a total volume that is even higher
315 than in the initial cold phase (Fig. 6e). This implies an inherent change of debris cover that comes with an abrupt change in ELA, given a fixed debris input rate and source.

Figure 7 summarizes the response in length and volume together with the corresponding e-folding response times. These e-folding response times quantify the time it takes for the glacier geometry to adjust by a fraction of $1 - \frac{1}{e}$ (about 63%) of change between the initial and final state after a step-change in forcing. Commonly, the response time refers to the adjustment
320 in volume (Johannesson et al., 1989; Zekollari and Huybrechts, 2015) but the concept of e-folding time can also be applied to the length adjustment (Oerlemans, 2007). We find that for our experiment the response times of debris-free and debris-covered glaciers to a step-change in ELA do not drastically differ. Length response is generally a bit slower than volume response in all cases, but the onset of length retreat of the debris-covered glacier is strongly delayed (40 yr), as previously observed by Ferguson and Vieli (2021). Nevertheless, the subsequent rapid retreat of the debris-covered glacier causes e-
325 folding response time to only be 18% slower than the debris-free response. The only exception is for the advance case, where the volume response is even shorter in the debris-covered case, which might be connected to the already more extended steady-state length before the advance. As mentioned above, the response to warming is also non-monotonic. The initial response in both length and volume first retreats beyond the final steady-state (Phase 2), then slowly re-advances to the final stable state
330 (Phase 3). When we include this slow rebounding phase in the calculation of the response time, we obtain values that are several times higher than the classic e-folding response time for retreat (Fig. 7b & c) and can be attributed to the timescale of transporting the debris through the glacier before it melts out at the surface. Finally, note that after reaching the final steady-state (Fig. 6d), resetting the ELA forcing to the initial value of 2900 m as before the warming, the terminus does not exactly return to its initial position and equilibrates in a slightly more elongated state. This effect is specific for this experiment and is discussed in detail in Appendix B1.

335 3.2.2 Step-change in debris input

We conduct a further step-change experiment where we vary the debris input rate instead of the ELA (Exp. deb-1), by decreasing d_{in} from 1 to 9 mm yr^{-1} and back while always keeping the ELA fixed at 2900 m. Figures 7 and B1 show advance and retreat after an increase or decrease in debris input rate respectively. Comparing the debris step-change experiment to the climate forcing experiment (Fig. 7), we find highly contrasting qualitative response behavior. Both glacier volume and length
340 show no reaction for about 300 years followed by very slow retreat or advance phases. Similarly, as in the slow rebounding Phase 3 in the ELA warming experiment, these highly delayed responses to debris input forcing are a result of the englacial transport times of the debris from input to melt-out. This transport of debris through the glacier and strongly delayed resurfacing on the glacier tongue is clearly visible in experiment deb-3, where brief (1 year long) spikes in debris input are deposited in the accumulation area every 1000 years (Fig. 8b). We can also observe the effect of these spike events in temporarily increasing

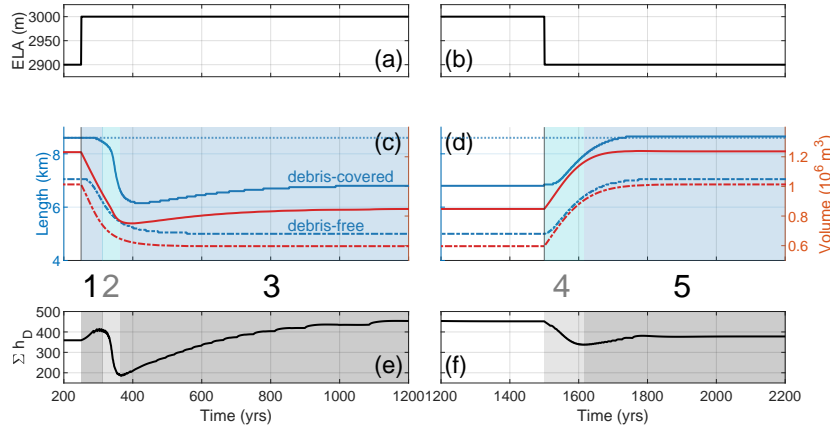


Figure 6. Experiment clim-1: ELA step-change experiments (Exp. clim-1) for (a) warming and (b) cooling with the related response (c & d) in debris-covered (blue solid line) and debris-free glacier length (blue dashed line) and glacier volume (corresponding red lines) and (e & f) total surface debris volume Σh_D . The shaded areas mark different phases (1–3 after warming, 4 & 5 after cooling) of length and debris cover response referred to in the text.

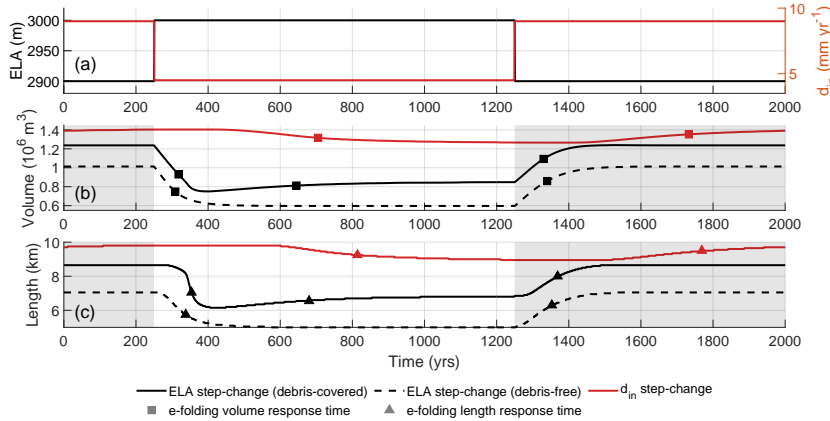


Figure 7. Experiments clim-1 & deb-1: Response times to a step-change in ELA (Exp. clim-1), for a debris-covered (black solid line) and a debris-free glacier (black dashed line), and to a step-change in debris input rate d_{in} (red solid line; Exp. deb-1): (a) forcing, (b) volume response and e-folding volume response times, and (c) length response and e-folding length response time. The symbols mark the time of reaching the response time (e-folding time) after the step-changes.

345 both debris thickness and glacier extent for over a hundred years (Fig. 8c).

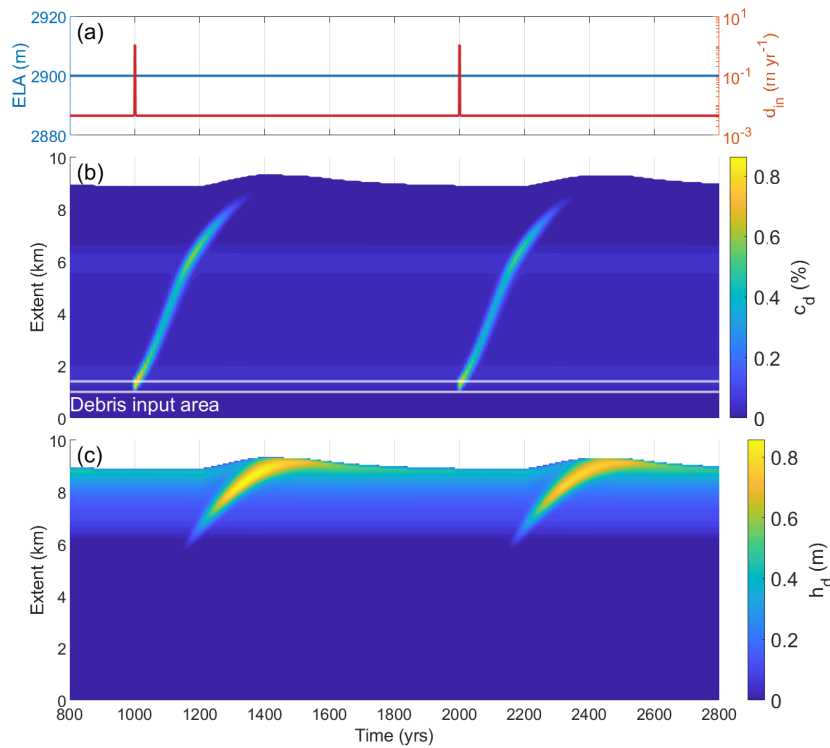


Figure 8. Experiment deb-3: Short-term debris input spike experiment (Exp. deb-3): (a) constant ELA and spike debris input rate forcing, (b) resulting depth-averaged englacial debris concentration over time and glacier extent, and (c) resulting debris cover thickness over time and glacier extent. During the spike event, 1 meter of debris is deposited on the glacier over 1 year. In the intermediate periods the standard debris input rate of 4.5 mm yr^{-1} is used.

Thus, beyond the generally slightly enhanced delayed response of debris-covered glaciers to climatic forcing, the additional delay when tracking englacial debris implies that a response to change in debris operates on a different, longer timescale than a response to climate. We observe a similarly long lag in Phase 3 (re-advance) in the debris-covered glacier response to warming 350 (Fig. 6c & 7). Similarly to the ELA experiment, we notice that there is a slight discrepancy between the final steady-state and initial state after a first cycle of debris input step-change (increase followed by decrease; e.g. Fig. B1), which is further explored in Appendix B1.

3.3 Transient response to periodic variations

In a next step of transient experiments, we examine how periodic variations in climate or debris input affect a debris-covered 355 glacier. For this purpose we periodically and separately vary the ELA with a sine function (amplitude = 100 m) or the debris

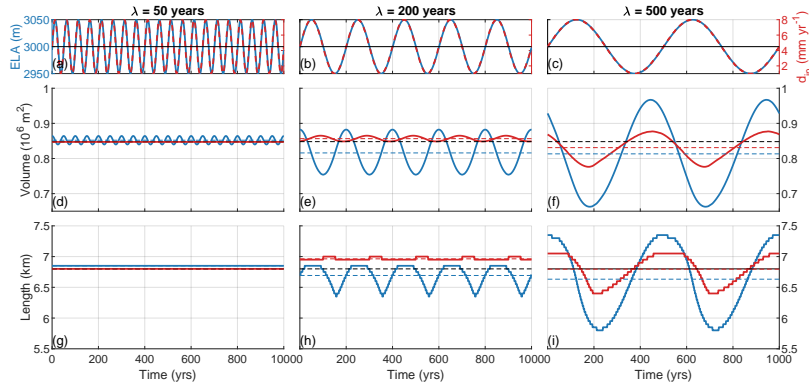


Figure 9. Experiments clim-3 & deb-2: Comparing glacier volume and length response to sine variations in climate (ELA, blue solid lines; Exp. clim-3) and debris input (d_{in} , red lines; Exp. deb-2) forcing with three different period lengths: (a,d,g) 50 years, (b,e,h) 200 years, and (c,f,i) 500 years. Dashed lines indicate volumes and lengths of a steady-state glacier (black) with the corresponding time-constant mean ELA and debris input rates, compared to mean volumes and lengths of the transient-state glaciers (blue and red lines).

input rate (amplitude = 7.0 mm yr^{-1}) around the reference values (ELA = 3000 m) and $d_{in} = 4.5 \text{ mm yr}^{-1}$; Fig. 9). Additional periodically transient experiments can be found in Appendix A. Generally, we observe that variations on timescales of

360 several decades (Fig. 9a) do not substantially affect glacier geometry, in particular in length, as long as there is no long-term background trend in the forcing. This is particularly true for variations in debris input, which do not seem to have any impact on the glacier length and volume on timescales below 200 years. In this case, even though debris thickness upstream might vary substantially over time, the glacier terminus is, within the grid resolution, almost stable.

Due to the effect of debris, the glacier geometry seems unresponsive to forcing fluctuations at timescales below a century and the glacier reaches a pseudo-steady-state. In contrast, for debris-free glaciers, the frequency of variations required to have 365 a significant impact on the glacier also depends on the glacier's response time, which itself can be impacted by a variety of factors such as glacier size, slope, and ice temperature (Johannesson et al., 1989; Bahr et al., 1998). In terms of quantitative effect on the glacier, changes in ELA seem much more impactful than changes in debris input. For example, in Figure 9, oscillating the ELA by just 100 meters has a larger effect on the glacier than varying debris input rates between 1 and 8 millimeters per year (multiple times). A variation of 100 meters roughly corresponds to 1 to 1.25°C (Lüthi, 2014), which is reasonable for 370 temperature variations in the Alps over the last millennium (Gosse et al., 2018).

3.4 Towards more realistic forcing

In this section, we aim to work towards more realistic debris-covered glacier behavior by exploring the effect of more complex climate forcing signals (Exp. clim-4) and bed topography (Exp. clim-5a/b) on a debris-covered glacier. While attributing the response to forcing might not be as direct as in the idealized cases above, these experiments include additional aspects such



375 as noisy forcing signals in a warming world or more variable along-flow variations in flow speed and debris thickness from undulations in bed topography.

3.4.1 ELA history forcing

Our climate forcing curves for experiment clim-4 (Fig. 10a) are based on data from two publications: Lüthi (2014) for the past 2000 years until the year 2020, Masson-Delmotte et al. (2021) for the following 1000 years into the future. The Lüthi (2014) 380 dataset reconstructs ELA history from alpine paleo-glacier variations over 2000 years until the year 2020. After 2020, we rely on temperature projections based on shared socioeconomic pathways (SSP). SSP1-1.9 (low emission), SSP2-4.5 (intermediate emission), and SSP5-8.5 (high emission) represent different scenarios of how global temperature may develop until the year 2090, based on projected changes in anthropogenic carbon emissions into the atmosphere. We use the best estimates for each scenario of temperature change until the 2081–2100 period (Masson-Delmotte et al., 2021) relative to the 1850–1900 reference 385 period. We assume linear temperature increase between the years 2020 and 2090 (the middle of the 2081–2100 period), followed by steady temperatures. We convert temperatures to ELA by multiplying with a sensitivity factor of 90 m K^{-1} (i.e. 90 m per degree temperature change) based on the estimate of $80\text{--}100 \text{ m K}^{-1}$ by Lüthi (2014). Finally, we add artificial decade-scale noise to the projected ELA curve (normally distributed, standard deviation matching the Lüthi (2014) data). Note, the debris 390 input area and rate are kept constant at 4.5 mm yr^{-1} . The chosen ELA history is not meant to be an accurate representation of real changes in climate or glacial response to it, but rather to provide representative temporal forcing patterns and trends in ELA for observed climates for the past millennia (medieval warm period, LIA cooling, decadal variations, future longer-term warming trends). Due to the observed long delays in response of debris-covered glaciers we start our forcing history at 1950 BCE (hereafter denoted as year 0).

395 Many of the observations made in previous experiments persist. Firstly and consistent with our earlier periodic forcing experiments, the short-term fluctuations in forcing (mostly from year 1500 onward) are filtered out in the volume and even more so in the length response (Fig. 10). Secondly, the retreat behavior during long warm or warming periods is similar to the step-warming case: a stagnating thinning tongue (Fig. 11c) followed by a rather abrupt retreat and ultimately slow re-advance through the build-up of a thick debris layer (Fig. 11b). However, we see that this re-advance and thick debris layer only appears 400 when the ELA remains roughly constant over multiple centuries (e.g. in the years 0 to 500 and 2100 to 3000 in Figure 11). During periods with high variability (decadal- to century-scales), the debris layers remain much thinner than during periods with near-constant climate (e.g. years 0 to 500, 2200 to 3000 in Fig. 11b). At the onset of warm periods and related stagnation and successive retreat, we observe that the flow speed and debris transport near the terminus is almost completely halted (Fig. 10c). Finally, the use of extreme climate scenarios (e.g. SSP5-8.5, the fossil-fueled society pathway from Masson-Delmotte et al. 405 (2021)) demonstrates well what happens when the ELA moves above the main body of the glacier and upstream of the debris deposition zone into the headwall. In this case, after the initial rapid retreat, the glacier keeps retreating extremely slowly, over hundreds of years. No rebound occurs here as the deposited debris always stays on the glacier surface and no delay from englacial debris transport occurs.

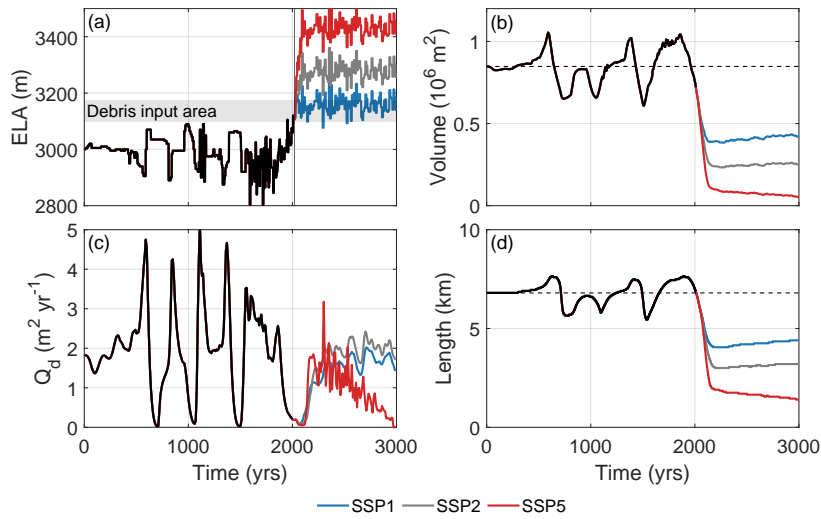


Figure 10. Experiment clim-4: Debris-covered transient response to complex climate forcing, based on a reconstructed climate history (Lüthi, 2014) and SSP1-1.9 to SSP5-8.5 climate scenarios (Masson-Delmotte et al., 2021) with synthetic short-term fluctuations: (a) ELA forcing, (b) volume response, (c) debris flux near terminus, and (d) length response.

3.4.2 Undulated bed topography

410 A last level of complexity is added when introducing a more realistic bed topography. For this, we utilize an elevation profile along a flowline of Zmuttgletscher, Switzerland, derived from a helicopter-borne ground penetrating radar (GPR) survey (Langhammer et al., 2019; Mölg et al., 2020) with 50m intervals. Figure 12 shows how this undulated bed and associated along-glacier variations in ice velocity (Fig. 13d) produce more variable debris cover patterns even in the initial steady state. Once we also apply the variable climate history (Fig. 13), an additional effect of complex topography appears: steep sections in the
 415 bed can cause detachment in phases of fast retreat, leading to stepped retreat and pockets of detached and stagnant ('dead') ice (see the 'overhanging' frontal margin around years 700 and 1450).

4 Discussion

We have presented a model that couples ice flow to en- and supraglacial debris transport and explored related feedbacks in various forcing setups ranging from simple stable states to complex transient responses. Here, we aim to discuss these findings
 420 to gain a better understanding of the debris–glacier system in a transient setting.

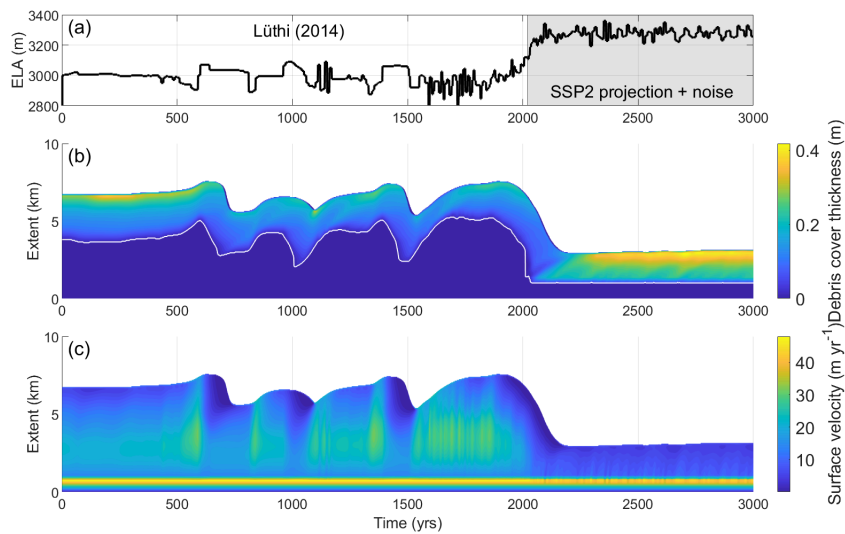


Figure 11. Experiment clim-4: Debris-covered transient response to complex climate forcing history: (a) ELA forcing derived from a reconstructed climate history (Lüthi, 2014) and SSP2-4.5 scenario (Masson-Delmotte et al., 2021) with superimposed synthetic short-term fluctuations, (b) debris cover thickness response, and (c) surface velocity response along the extent of the glacier. The white line in (b) marks the first grid point where debris thickness > 0.01 m, i.e. where debris starts emerging.

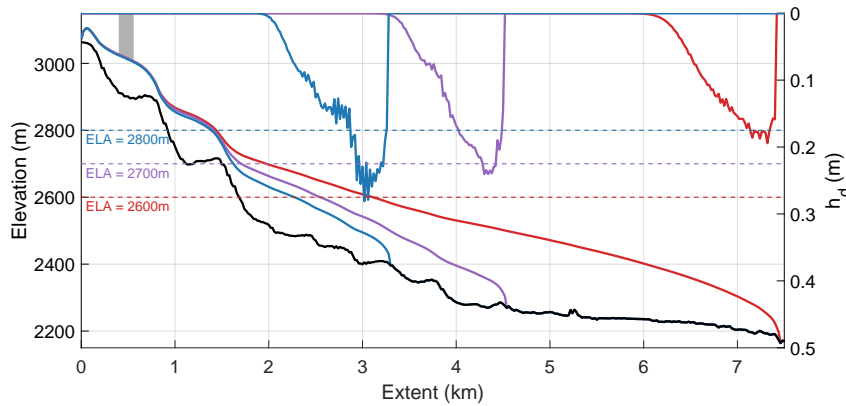


Figure 12. Experiment clim-5a: Influence of an undulated topography on steady-state glacier geometry: three steady-state glaciers (at ELAs of 2600, 2700, and 2800 m a.s.l.) and corresponding debris cover thickness (inverted scale, 0 at the top) on a bed topography adapted from Zmuttgletscher, Switzerland.

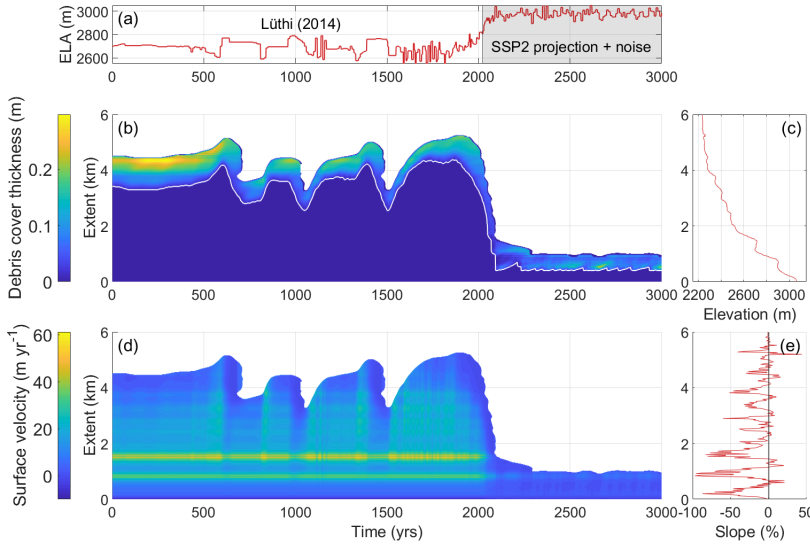


Figure 13. Experiment clim-5b: Debris-covered transient response to complex climate forcing on an undulated bed topography: (a) ELA forcing derived from reconstructed climate history (Lüthi, 2014) and SSP2-4.5 scenario (Masson-Delmotte et al., 2021), (b) debris cover thickness response, (c) along-glacier bed elevation, (d) surface velocity response over the extent of the glacier on a Zmuttgletscher-like bed topography (Fig. 12), and (e) along-glacier bed slope. The white line in (b) marks the first grid point where debris thickness > 0.01 m, i.e. where debris starts emerging.

4.1 Response to transient climate

In our transient climate forcing experiments (Exp. clim-1 to clim-5) we compare debris-free and debris-covered response in retreat and advance. Similar experiments were already conducted in Ferguson and Vieli (2021) with a simpler version of the model that does not include heterogeneous englacial debris transport. They also observe a delayed retreat response to warming 425 connected to thinning behavior. Here, we characterize the transient debris-covered glacier response when including englacial debris-transport.

After warming, a debris-free glacier instantly starts both retreating and thinning (Fig. 6) because mass balance decreases, roughly linearly, towards the terminus (Fig. 4b), causing the lowest parts of the glacier to melt fastest. Conversely, debris cover thickness of a debris-covered glacier increases towards the terminus and ablation is suppressed there (e.g. Fig. B3b & 4c), 430 leading to a flat or even inverse mass balance gradient (Fig. 4b) and a stagnant terminus position, which have both been observed on real glaciers (Nakawo et al., 1999; Benn and Lehmkuhl, 2000; Benn et al., 2012; Thompson et al., 2016; Ragettli et al., 2016; Rounce et al., 2018; Mölg et al., 2019). One direct consequence of this flat mass balance gradient is the tendency of debris-covered glaciers to exhibit stagnation and thinning along the ablation area rather than terminal retreat in the first few decades of warming (Banerjee and Shankar, 2013; Ferguson and Vieli, 2021).



435 After this stagnating and thinning phase under warming (Phase 1), the debris-covered glacier abruptly retreats (Phase 2),
436 accompanied by the loss of large parts of the supraglacial cover within decades (Fig. 6). During this period, debris flux is
437 temporarily decreased in the ablation area (e.g. Fig. B3c), which has implications on studies relying on debris flux or other
438 transport metrics to infer debris supply rates (McCarthy et al., 2022). As the glacier completes its dynamic adjustment to the
439 change in climate, retreat comes to a halt. Subsequently, a slow process of debris cover recovery and subsequent re-advance
440 begins (Phase 3), which has not been documented in any other study. Debris cover rebounds for two distinct reasons: firstly, the
441 now shorter englacial trajectory (further discussed in Sect. 4.4.1) that leads to melt-out of debris further up-glacier. Secondly,
442 ice mass turnover is reduced under the new warmer conditions, while the debris supply remains constant. This change in debris
443 to ice ratio manifests in higher debris concentrations that only lead to a noticeable change in debris thickness after a lag period
444 of englacial transport (Video Supplement 1), further discussed in Sect. 4.3). As the higher debris concentration reaches the
445 ablation area and melts out, debris flux approaches its balanced quantity again (e.g. Fig. B3c), corresponding to the supply rate
446 up-glacier. In the new warmer steady-state, the lower velocities counter-intuitively lead to higher total amounts of supraglacial
447 debris in steady-state, even after retreat. However, this recovery takes hundreds of years, meaning, it is difficult to show or
448 validate this newly discovered effect in experiments or observations under a climate varying on shorter timescales.

450 This is explored in the experiments (clim-4) applying a more complex climate with large variability on the scale of multiple
451 decades to single centuries (Fig. 11b & 9c). Under such forcing, debris cover is regularly removed in phases of sustained
452 warming and hence retreat (centuries), and by the onset of debris cover recovery, the climate is in most cases already changing
453 (cooling) again, leading to thinner debris cover compared to an averaged constant climate. This leads us to the conclusion that
454 long-term climate variability with phases of prolonged warming overall suppresses the formation of thick supraglacial debris
455 layers that would be possible in steady-state or pseudo-steady-state climates. Ferguson and Vieli (2021) observed the opposite
456 effect in their century-scale random climate experiment when using a homogeneous englacial debris concentration. This may
457 be due to differences in experimental setup but could also indicate that incorporating depth-resolved englacial transport has a
458 significant influence on the transient response.

460 During longer warm periods, debris transport near the terminus is almost completely halted (Fig. 10c) due to stagnation
461 in ice flow. This leads to the debris layer not being transported off-glacier and only increasing in thickness through more
462 debris melt-out while the ice is thinning. Dynamically stagnant tongues have been observed on many debris-covered glaciers
463 (e.g. Thompson et al. (2016)), but here we show new implications on temporal variations in debris transport and export from
464 the glacier. Conversely, cooling leads to immediate acceleration of the ice (Fig. 11c) and therefore much faster debris transport,
465 accompanied by instantaneous re-burial of any surface debris that is now above the ELA (advance of zero debris thickness line
466 in Fig. 11b). The use of extreme scenarios (e.g. SSP5-8.5) illustrates the impact from an ELA moving above the main body
467 of the glacier and behind the deposition area into the headwall. In this case the long-term re-advance trend vanishes as the
468 ablation area of the glacier is no longer supplied with englacial debris (Fig. 10). This switch in long-term response is driven by
469 the ELA crossing a threshold which is likely related to the location of debris input or, in a natural system, by crossing the foot
470 of the headwall. This configuration of ELA and debris source in a model, combined with an avalanching mechanism, might
471 also be able to represent rock glaciers (Anderson et al., 2018).



470 Further sensitivity experiments (see Appendix C) show that the general findings in transient behavior are robust and qualitatively indistinguishable to deviations in Glen's flow law parameter A (Fig. C1). Variations in the Østrem curve (parameter D_0) (Fig. C3) show a stronger impact on warming response. Specifically, a higher value of D_0 (weaker effect of debris on ablation) leads to faster, but less abrupt retreat and a less pronounced rebound, essentially exhibiting retreat more similar to debris-free glaciers. Fontrodona-Bach et al. (2025) compiled all available debris thicknesses and related ablation rates and
475 show a wide spread in D_0 and a mean value (0.061 m) very similar to our default value (0.065 m), emphasizing the need for models to either constrain D_0 for individual glaciers or address the large uncertainty when using a standard value. A further major assumption that might impact transient behavior concerns the boundary condition at the glacier terminus. There, we assume the presence of a terminal ice cliff. Our implementation is a crude approximation of real terminal ice cliffs as observed at some debris-covered glaciers (Nainwal et al., 2016; Mölg et al., 2019). However, terminal morphology varies strongly between
480 debris-covered glaciers (Rowan et al., 2015) and is not completely understood. The absence of an ice cliff might lead to much more stable terminus position. However, the processes leading to a specific terminus type are not currently well-understood, forcing us to assume terminal conditions.

485 The linear relationship between debris input and dELA described in Sect. 3.1.2 (Fig. 5a) suggests that an increase in debris input can compensate linearly for a warmer climate. Anderson and Anderson (2016) describe a similar relationship, but related steady-state glacier size to debris flux. However, in a transient state, debris flux is a product of debris input and ice dynamics. A dynamically induced increase in debris flux would actually lead to a more efficient evacuation of debris, causing thinner debris thicknesses and decreasing the protective effect of debris. Therefore, we argue that using absolute debris input in this context is more appropriate, as it disentangles observations from ice dynamics influence. The observation that dELA is independent of ELA (Fig. 5b) means that a fixed debris input will compensate the same ELA difference at any elevation, given a flat bed
490 topography and an ELA-independent debris input rate. Some studies suggest that warming may cause increased paraglacial rockfall activity, either directly from an increase in frost-cracking (Banerjee and Wani, 2018) or indirectly through deglaciation of rockwalls and the onset of weathering following surface exposure (Hartmeyer et al., 2020). Under this assumption, increased debris supply might help mitigate warming-induced retreat. In conclusion, our results regarding debris input and glacier geometry match with previous modelling approaches. The effect of a constant debris source on glacier size is elevation-independent,
495 but literature suggests that our assumptions regarding this source might be inaccurate.

4.2 Response to transient debris input

500 In our experiments with transient debris forcing (Exp. deb-1 to deb-3) we are able to characterize glacier response to a variable debris source. While past approaches assumed debris supply to be steady in space and time (Anderson and Anderson, 2016; Ferguson, 2022), the stochastic nature of gravitational processes and potential feedbacks with deglaciation (Banerjee and Wani, 2018; Hartmeyer et al., 2020) motivate our examination of spatially and temporally transient debris input. As described in Sect. 3.2.2, the response to changes in debris input often operates on a longer timescale than to changes in climate (Fig. 7). This is mainly a result of the required time of englacial debris transport from the source to the melt-out area, as nicely visible in Figure 8b. Consequently, this 'debris advection response time' highly depends on the position of the source in relation to the



ELA. Long englacial pathways in a system where debris is added to the glacier high above the ELA lead to a slow response, 505 both because of increased transport distance and decreased ice velocity in the lower parts of the ice column. Of course, the dynamic state of the glacier (mass turnover) is also relevant in a general sense, as a highly dynamic (e.g. fast flowing or advancing) glacier responds more quickly than a stagnant glacier.

Periodic (Exp. deb-2; Fig. 9) and random short-term (10 yr) variations (Video Supplement 2) show that variability in debris input, in the absence of any longer-term trend, barely affects the glacier length evolution even on a century timescale. This 510 shows that the debris-covered glacier system is insensitive to short-term fluctuations in debris input, unless the debris input occurs onto the ablation area or an isolated event several orders of magnitude larger than the long-term mean occurs (Fig. 8). Note that in the latter, depending on the englacial trajectory, the length-response can be delayed by several centuries (Vacco et al., 2010). At longer timescales (500 year wavelength), the response exhibits a phase shift of half a period, leading to a seemingly inverse relationship between debris input and glacier volume. This strongly supports the notion that recent changes 515 in debris supply to the accumulation area are not readily apparent in observable variations of down-glacier debris cover patterns, thereby contributing to the complexity of the debris-covered glacier response. Approaches to infer long-term debris supply rates from debris cover (e.g. McCarthy et al. (2022)) might profit from this smoothing process that should roughly average supply rates over several centuries.

4.3 The role of debris dynamics in the debris-covered glacier response

520 As illustrated in sections 3.2 and 4.2, we find that responses of debris-covered glaciers operate on multiple interfering timescales. While delayed retreat has been described in earlier studies (Ferguson and Vieli, 2021; Ferguson, 2022), we disentangle the complex response into tangible process interactions between debris transport and glacier mass balance. Post-warming volume loss (Fig. 6 or 7) shows that changes in ELA impact surface mass balance instantly, whereas any change to debris input in the accumulation area is transported englacially and can only take effect after it emerges at the surface in the ablation area. The time 525 the debris cover thickness takes to fully adjust to a change in ELA during the post-retreat rebound phase is similarly long as the response to a change in debris input. It is also a direct consequence of englacial transport of newly higher debris concentrations. This concentration increase is a result of lowered ice accumulation in a warmer climate while absolute debris input remains constant (further explored in Sect. 4.4.1). Consequently, any change in debris concentration in the input area requires centuries 530 to affect the glacier, irrespective of the underlying cause, whether it pertains to variations in debris input or ice accumulation. The duration of this lag is dependent on debris supply amount and most importantly debris input location relative to the ELA. This advection timescale becomes increasingly relevant when debris is deposited on the glacier in the accumulation area with increasing distance to the ELA. Further, the relative importance of the debris advection lag depends on ice dynamics, or more simply on glacier size. While increased ice velocities in larger glaciers lead to accelerated debris advection, small glaciers may have lower mass turnover, but generally shorter debris transport paths. As these effects counteract each other, the constellation 535 of debris input area and ELA, given by local conditions, is much more relevant to response times. Assuming homogeneous debris concentrations (Rowan et al., 2015; Ferguson and Vieli, 2021) or positioning the debris supply at the margins (Margirier et al., 2025) risks over- or underestimation of the resulting debris cover, respectively.



The lag related to englacial transport further contributes to the attenuation of any debris input signal when observing debris cover. For example, a measured increase in debris concentration can either originate from increased debris supply or decreased 540 ice accumulation at the time of formation. As such, this equifinality contributes to the complexity of inverting from debris cover thickness distribution to past debris input rates or historic climate states. In addition, once the debris has reached the surface in the ablation area, debris redistribution processes (Kirkbride and Deline, 2013; Moore, 2018; Bartlett et al., 2021; Ferguson, 2022) can smooth out or create new variations in along- and across-glacier debris distribution. For natural glacier 545 systems with multiple debris sources that are variable in amount and position, have a sporadic record of debris cover, a variable climate history, and debris re-distribution such reconstructions become ambiguous if not impossible.

Reflecting on debris thickness measurement strategies, we can conclude that more extensive records of current debris cover might only marginally improve estimates of past debris input or climate. The long timescales involved in debris transport, as well as the fact that any measurement on debris-covered glaciers is constrained to our current period of warming, lead 550 to an inherent observational bias (Ferguson and Vieli, 2021). Our modelling experiments enable us to evolve debris-covered glaciers in any climatic setting and over long timescales. Our results show that the relative positions of debris source and ELA are highly relevant to the extent of debris cover that influences glacier volume and extent. Within the debris-covered area, small-scale variations can rarely be traced back to a single source.

4.4 Transient debris-climate feedbacks

We have presented a multitude of transient experiments on a modelled debris-covered glacier, where we made observations 555 about feedbacks in the system related to debris. Here we aim to discuss these feedbacks and the glacier system states resulting from them.

4.4.1 Englacial trajectory feedback

We have observed that a shift to a warmer climate leads to more debris being at the surface than in a cooler state (Fig. 6) if debris input occurs in the accumulation area. We can identify several processes leading to this debris cover increase.

560 Firstly, englacial trajectories are shortened as warming moves the ELA closer to the input area, similarly to when we move the position of the debris input area. This means debris spends a larger portion of its transport path on the glacier surface instead of englacially, decreasing mass balance. While the initial expansion of debris cover (increase in total debris in Fig. 6e) can be attributed to melt-out of pre-existing englacial debris within the ice as the glacier surface lowers, the permanent up-glacier shift of the debris cover is a consequence of this reduction in englacial path length (Video Supplement 1). The opposite effect 565 applies to a glacier where debris is deposited onto the ablation area: warming causes the ELA to move away from the input area, causing a larger area above the debris input area (in the ablation area) to be debris-free, which increases melt. During intense and prolonged warming, a glacier might transition from depositing debris onto the accumulation area to depositing directly to the surface in the ablation area. We conclude that the shorter the distance between debris input area and ELA, the larger the debris-covered area and, consequently, the stronger the protective effect. Anderson and Anderson (2016) have 570 previously described this relationship in their approach, further tying maximum debris cover extent to the proximity of debris



input to maximum ice flux (at the ELA). This certainly holds true in steady-state but not in transient conditions, as ice and debris dynamics have different response times.

Secondly, ice velocities are lower for a thinner, shorter glacier corresponding to a warmer state. To satisfy debris mass conservation in the long-term, debris needs to be exported from source (debris input area) to sink (terminus) at a constant rate.
575 For a glacier in balance, debris flux is constant along the entire glacier in a steady-state, which results in thicker debris in a warmer state. This effect applies independent of the relative position of the debris input area, as it entirely depends on changes in velocity.

Thirdly, as the system transitions towards a new equilibrium after warming, debris concentrations in the debris input area increase immediately. Englacial transport leads to a lag in response to this increase (see Sect. 4.3) that depends on the new
580 relative position of the debris input area and ELA. After englacial transport and melt-out, the increased concentrations lead to further increase in debris thickness.

We summarize that, irrespective of whether local mass balance is positive or negative in the debris input area, the relative position of debris input to the ELA is highly relevant to the ablation reduction effect of debris in the ablation area, which increases as the two get closer. While warming leads to an increase in local debris thickness in all cases, expansion of the
585 debris-covered area is limited to glaciers with debris input onto the accumulation area. Debris supply to the ablation area from unstable moraines, rockfall, or avalanching (van Woerkom et al., 2019; Stewart et al., 2025), where subsequent debris transport is exclusively supraglacial, may substantially contribute debris to the surface and lead to overestimation of expansion potential Herreid and Pellicciotti (2020).

4.4.2 Topography feedback

590 Basal topography strongly impacts glacier geometry (surface slope and ice thickness), especially for debris-covered glaciers. Slopes are usually steeper where surface debris is absent (in the accumulation area) and flatter where it is present (Sect. 3.4). Due to the inversely proportional melt reduction effect from debris thickness, steep topographic steps lead to enhanced melt-out of debris, which is rapidly propagated into the flat parts. There, the combined effect of flat terrain and debris-reduced
595 ablation can further exacerbate the formation of elongated, low-velocity tongues on the flat valley floor. In nature, this effect may be further enhanced when considering the process of debris mobilization or removal through slope movements in very steep parts (Moore, 2018; Westoby et al., 2020; Mayer and Licciulli, 2021), a process that is not included here.

Under a transient forcing, a more realistic, undulated bed topography based on a real glacier bed (Exp. clim-5; Fig. 12 & 13) can cause additional effects: (i) during a warming phase, the flat debris-covered parts with a concave bed can detach (Pellicciotti et al., 2015; Rippin et al., 2020; Rowan et al., 2021) from the steep sections just upstream, as melt rates are, due to the thinner debris, much higher there and the ice is already thin (compare Figure 13 to Figure 11). (ii) The concave shape of the bed favors elongated glacier shapes where small differences in ELA have a larger impact on the glacier. This means both more mass gain in advance and more mass loss in retreat, but favoring the elongated state because of the asymmetry between instant advance and delayed retreat discussed in Sect. 3.2.1.



4.5 Limitations

605 While our implementation of debris input and transport is close to achieving consistent debris mass conservation independent of climate, it still fails under certain circumstances. When debris is deposited too close to the ELA (Appendix B2) the model systematically underestimates debris cover. Consequently, the model is not fit for all combinations of climate and debris inputs. However, we have designed our experiments to minimize the impact of this inconsistency by avoiding parameter ranges where results are unreliable, thoroughly investigating issues, and focusing on relative results. This approach substantiates our
610 confidence in the robustness of the results obtained.

615 A second intrinsic model issue is an inconsistency related to model spin-up. Depending on if a desired initial state is spun up from a less (e.g. debris-free) or more debris-covered state, terminus position will vary by a few grid points (Fig. B1; Appendix B1). The same issue leads to minor discrepancies between terminus positions before and after a phase of warming or increased debris supply. As all our model runs are spun up identically from a debris-free state, we do not expect this to affect our results strongly. The issue is most likely connected to the implementation of the terminal boundary condition and is discussed in more detail in Appendix B1.

620 We consciously simplify the complex surface processes by using a single Østrem curve, which would ideally be unique to any glacier and is in itself a strong generalization of the complex impact of debris on the energy balance. Our sensitivity analysis shows that the ablation reduction effect of debris cover is sensitive to D_0 , for which a wide range of values is found in literature (Fontrodona-Bach et al., 2025), both quantitatively and in terms of transient behavior. For this reason, we believe constraining D_0 for individual glaciers is important to understanding their current and future behavior through modelling.

625 With respect to model forcing, our implementation of a narrow, constrained debris input area with a usually constant debris supply is based only on rough estimates for erosion rates from literature (Anderson and Anderson, 2016) and an assumption of where debris would likely be deposited on the glacier. Future approaches could constrain debris supply position by relying more on records of rockfall deposits or relating debris supply spatially to surface properties such as slope. Additionally, future approaches could improve models by parametrizing surface processes such as debris re-distribution, the formation and impact of ice cliffs, or the formation of terminal ice cliffs and conduit collapses.

5 Conclusions

630 We present a glacier flow-model that explicitly tracks englacial debris transport and enables temporally and spatially varying debris supply under a transient climate forcing, thereby improving significantly on previous approaches. Our implementation of debris supply as an independent forcing variable allows direct comparison between debris supply rates and observed downstream debris concentrations and thickness patterns. We also assess the numerical robustness and explore the capabilities of this model. In a second step, we exploit these new capabilities by conducting a set of experiments to make some general observations about the dynamics of debris-covered glaciers and extract a number of robust findings:



635 – Debris-covered glacier response to warming in our model is distinctly different from debris-free retreat, being segmented into three clear phases: stagnation, retreat, and long-term re-advance. The non-monotonic response can be attributed to the differing response times of ice and debris.

640 – The prolonged response time of englacial debris transport and the discrepancy with glacial volume response time make reconstruction of past variations in climate or debris supply inherently ambiguous, unless one of the two remains more or less constant.

645 – Low-amplitude, short-term (decade-scale) variability in climate and in particular debris input have been demonstrated to have a negligible impact on glacier geometry. Conversely, high-amplitude events that supply large quantities of debris can exert a significant and sustained impact on the glacier but only over long timescales.

650 – Debris flux (and thus debris transport) is only constant over time and along the glacier when the system is in steady-state, which in nature does not really occur. During retreat, there is a temporary deficit in debris flux leading to a debris thickening, while advance causes a temporary debris flux surplus.

655 – When transitioning from a colder to a warmer state, the reduction in length of englacial debris trajectories and decreased ice velocities result in an increase in the debris-covered area fraction and a thickening of debris cover.

– Characteristically concave steps in bed topography favor the detachment of elongated debris-covered tongues, accelerating the retreat process.

– Long-term climate variability suppresses the formation of thick supraglacial debris layers that would be possible in steady-state or pseudo-steady-state climates.

– While debris cover leads to an elongated steady-state geometry, it only minimally affects up-glacier dynamics. The length of a glacier is linearly proportional to the quantity of debris supply, even though the increase in the protective effect diminishes for thick debris. The proximity of the debris input location to the ELA influences total debris-covered area and length of the glacier.

660 In summary, we have found sophisticated feedbacks involving debris and ice dynamics, where debris-related processes operate on several separate timescales. This leads to a complex transient response to changes in climate in multiple distinct stages. Our result show the expansion and thickening of debris cover caused by warming, as observed on many glaciers in the world, enabling re-advance after warming-induced retreat. We show that disentangling debris-covered glacier systems with multiple unknown variables and differences in response times is difficult. Yet short-term variability in forcing has only minimal impact on glacier extent, thereby rendering changes in the state of debris-covered glaciers more indicative of long-term trends than individual disturbances, even more so than for debris-free glaciers.



665 *Code and data availability.* The model presented in this study as well as the code and synthetic data (generated from model runs) will be up-
loaded to Zenodo once the paper is accepted and is currently available for reviewers here: <https://drive.switch.ch/index.php/s/B389m5dqdmeh9qa>

666 *Video supplement.* Two animations, referenced in the text as Video Supplement 1 and 2, have been uploaded here for reviewers and will
published on Zenodo once the paper is accepted: <https://drive.switch.ch/index.php/s/rMjOoGwwqeK4Bq5>

Appendix A: Additional time transient modelling experiments

667 Below, two additional experiments of time transient forcings in debris and climate input are presented. Figure A1 shows the
effect of a long-term (century-scale) fluctuation in debris input position. Similarly to the steady-state case (Fig. 4), we observe
a relationship between along-flow position of debris input and the extent of the down-glacier debris covered area. Unique to
the transient case is a large variation near the terminus, connected to dynamic stagnation (Fig. A1b) whenever debris cover
decline leads to lower mass balance.

675 Figure A2 compares debris-free and debris-covered glaciers in their transient response to oscillations in ELA. By comparing
glaciers with equivalent (steady-state) volume, we can account for other dynamic effects on the response and show that debris-
covered glaciers are less reactive than debris-free glaciers of comparable size, both in volume (Fig. A2b) and length (Fig. A2c).

Appendix B: Model robustness and parameter sensitivity

680 In this section, we conduct experiments to test the robustness of the model performance in transient behavior, using strongly
idealized setup and parameters. This includes the examination of model sensitivity to parameter variability on an individual
basis. We further explore and discuss aspects of the model in terms of long-term reversibility when returning to the initial
forcing state (Appendix B1) and debris flux conservation (Appendix B2).

B1 Model reversibility

685 As noted in sections 3.2.1 & 3.2.2, steady-state terminus positions can slightly differ for identical parameter sets based on
previous states. Experiments clim-1 and deb-1 (Fig. 6, B1 & B2) show that reaching a steady-state from a previously more
debris-covered state (higher ELA or d_{in}) leads to a slightly more advanced terminus position than in the previous less debris-
covered state. The discrepancy is more enhanced (400 m) in experiment deb-1, where we directly affect debris cover by altering
the debris input quantity, in comparison to the ELA change experiment clim-1 (50 m), where the impact on debris cover is
indirect through a change in accumulation rate, while keeping the total debris input rate the same (Fig. B3). In the latter case,
a glacier carries more total debris on its surface when in a warmer state (Fig. 6e & f).

690 We further explore the range of possible states (Fig. B1) for a single set of parameters, which shows the resulting length for
a wide variety of temporary d_{in} step-change magnitudes (a) and durations (b). For both amount and duration we see a slight
increase in post-event steady-state length, confined by a maximum length, which seems to represent the longest glacier that

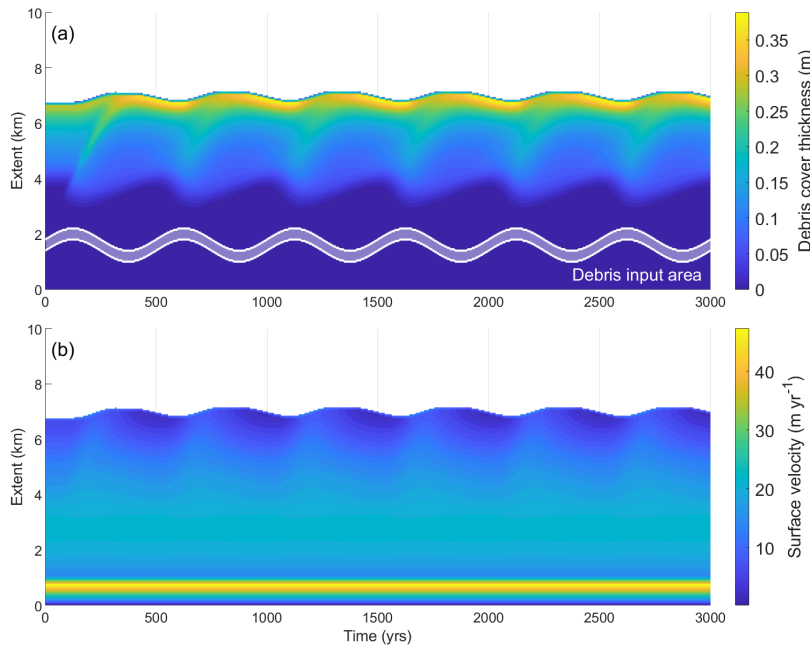


Figure A1. Varying debris input position in a sine wave (wavelength = 500 years, amplitude = 800 m with $1000 \text{ m} \leq x_d \leq 1800 \text{ m}$, ELA = 3000 m). (a) Debris cover thickness response and (b) surface velocity over time and along-glacier extent.

can be sustained with this particular steady-state set of forcing variables. Conversely, coming from a less debris-covered initial state will always result in the minimum stable state (red line in Fig. B1a & c), and hence is reversible, even if preceded by a
 695 more debris-covered state.

To further investigate whether this discrepancy is purely a numerical issue arising from the implementation of the terminal boundary condition (as described in Sect. 2.5), we conduct an additional experiment. The ice cliff thickness parameter H^* , otherwise considered a model parameter fixed at 30 m, is in this experiment oscillating as a sine wave between 10 and 50 m at a decadal time-scale ($\lambda = 40 \text{ yr}$, emulating a cyclically forming and collapsing terminal ice cliff). In this configuration, debris
 700 is removed more efficiently at the terminus, leading to a generally less elongated steady-state glacier after retreat. Our results (Fig. B4) suggest that, even with large variations in cliff height, the difference to the initial state, though more subdued, persists. Still, the debris cover profiles (Fig. B4b) are only distinguishable between the initial and elongated states in the immediate vicinity of the terminus, leading us to the conclusion that the discrepancy is most likely connected to the terminal boundary implementation and not an observable dynamic feedback.

705

Overall, our results emphasize that the modelled steady state glacier length is in our modelling strictly speaking not reversible and dependent on the previous state of debris cover, but in our experiments the effect stays small (a few percent) and impor-

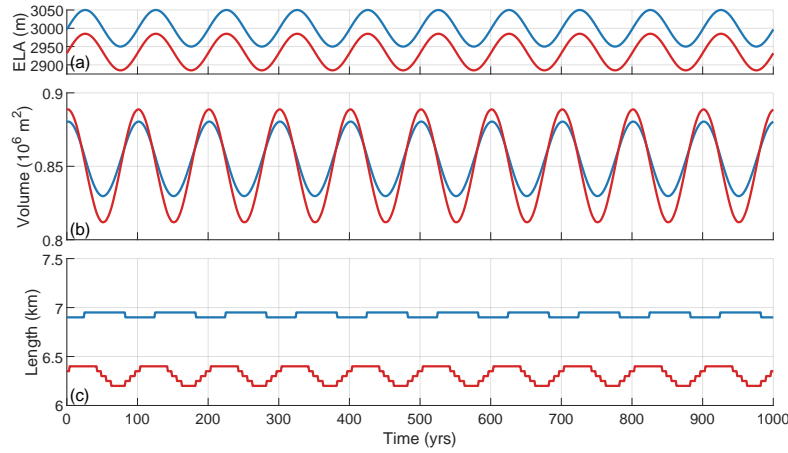


Figure A2. Sine wave climate experiment comparing a clean-ice (red) to a debris-covered (blue) glacier. (a) ELA oscillating with an amplitude of 50 m and $\lambda = 100$ yr around 2935 (clean-ice) and 3000 m a.s.l. (debris-covered). This corresponds to equal steady-state volumes, enabling a direct comparison of dynamic response: (b) glacier volume and (c) length response.

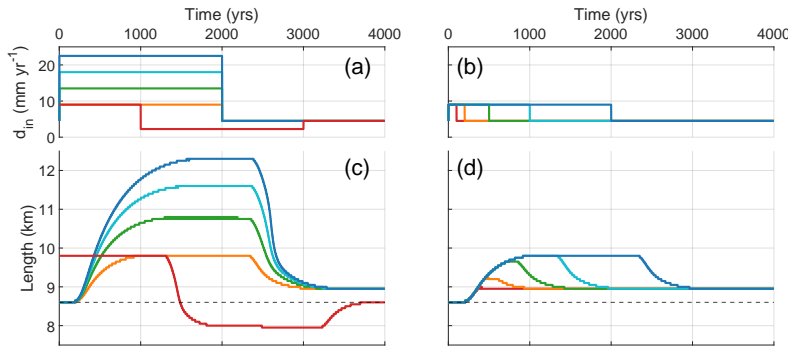


Figure B1. Debris input step-change experiments deb-1: (a) increasing d_{in} at time zero from 4.5 mm yr^{-1} to double (orange), triple (green), quadruple (cyan), quintuple (blue), as well as doubling followed by halving (red) after 1000 years. After 2000 years the debris input is reset to the initial value. (b) Varying duration of debris input doubling d_{in} experiment: 100 (red), 200 (orange), 500 (green), 1000 (cyan), and 2000 years (blue). (c,d) Corresponding glacier length responses.

tantly it only affects the debris thickness and glacier geometry in the terminal few hundred meters. Furthermore, in nature climate is rapidly fluctuating and this steady-state effect not really observable. For consistency in our modelling experiments we always start our experiments with the minimum steady-state as initial condition.

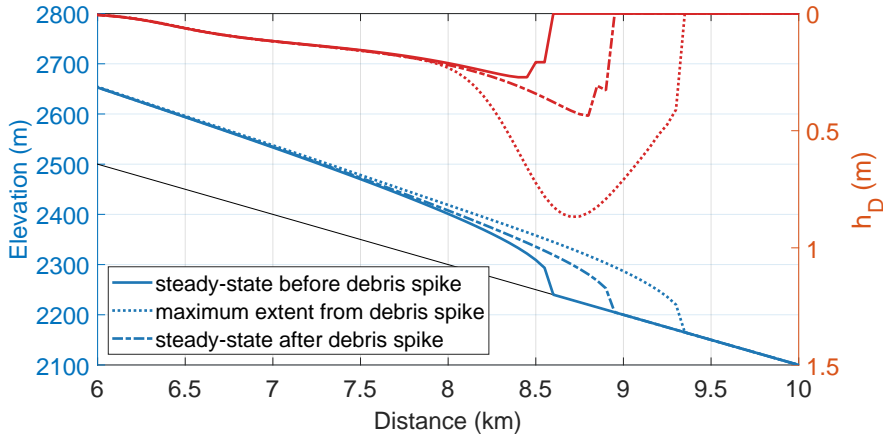


Figure B2. Geometry adjustment in short-term debris input spike experiment (Exp. deb-3; Fig. 8): glacier geometry (blue) and debris cover thickness (red) at three relevant points in time: at the steady-state before the first spike event (solid lines), at maximum extent caused by the spike (dotted lines), and at the new steady-state after the event (dashed lines).

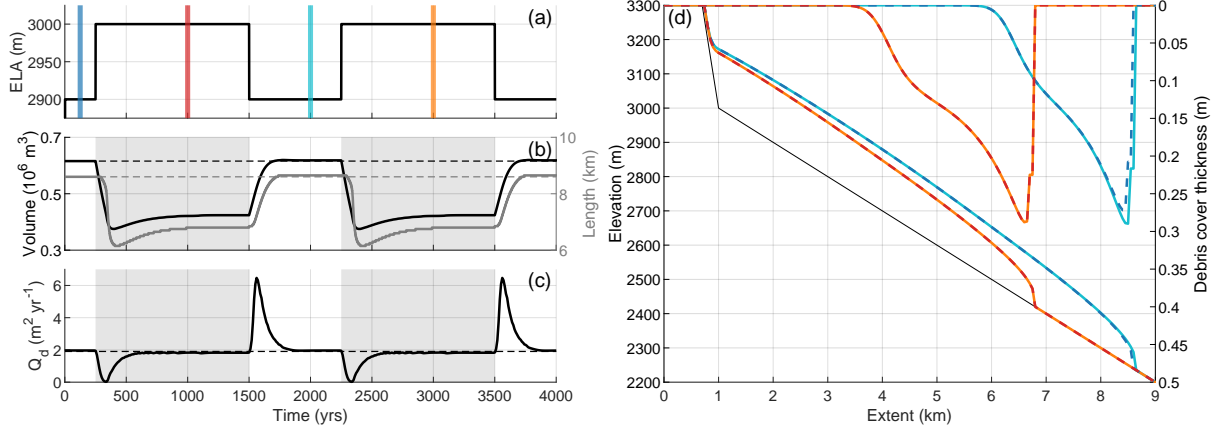


Figure B3. Repeated 100 meter ELA step-change experiment: (a) ELA forcing and markings for the four steady-states shown in (d). (b) Glacier volume and length response, (c) near-terminus debris flux response. (d) Four steady-state glacier geometries as marked with the colored bars in (a), at 2900 m (blue, cyan) and 3000 m (red, orange) ELA.

B2 Debris mass conservation

In Figure B5 we examine the along-glacier debris flux Q_d , spatially resolved, for a set of steady-states with ELAs ranging from 2700 to 3200 m. As long as the debris input zone is well above or well below the ELA (here: debris input occurs roughly between 3100 and 3175 m, hence for ELAs from 3000 m downwards or 3200 m upwards), the total debris flux, consisting of

715 the sum of englacial and supraglacial flux, is almost constant and conserved within a few percent along the glacier. However,

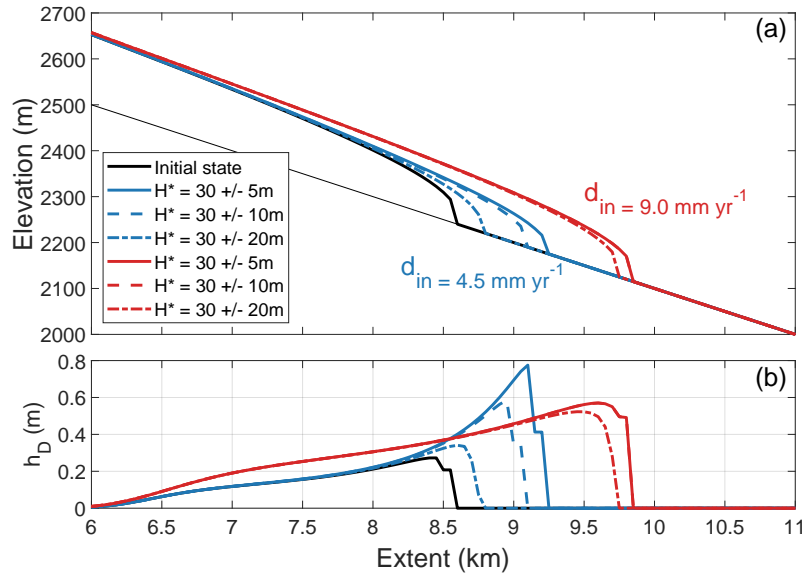


Figure B4. Influence of variable terminal cliff height H^* on terminus position relative to the initial (undisturbed) position: (a) geometry of the debris-covered ablation area for the following cases: initial steady-state (black), advanced, d_{in} -enhanced steady-state (red), and post-advance state with the initial standard parameter set (blue). The disturbances are implemented as sine waves in H^* ($\lambda = 40 \text{ yr}$) with amplitudes of 5 (solid line), 10 (dashed), and 20 (dash-dotted) meters, respectively. (b) Along-flow debris thickness profile of the cases described in (a).

as soon as the ELA is at a similar elevation as the debris input zone (e.g. 3100 m) the debris flux is substantially reduced (by about 35%), which means debris is lost. This issue is restricted to the specific case where debris is deposited onto the glacier in close proximity of the ELA, which is rarely the case in our experiments. Smaller discrepancies like slightly lower debris flux whenever englacial debris is involved can be attributed to numerical diffusion.

720 **Appendix C: Sensitivity to standard model parameters**

For Glen's flow law rate factor A and the characteristic debris thickness D_0 , both assumed as constant model parameters in our experiments, we found a range of values in literature. These parameters also depend on conditions like ice temperatures or lithology and should be constrained by empirical evidence when modelling a specific glacier. Here we examine the impact in transient response from a sensible range of model parameters based on the literature (Anderson and Anderson, 2016; Ferguson and Vieli, 2021) and empirical data (Fig. C2). The sensitivity of the transient model response to these variables was tested in a standard ELA step-change experiment (clim-1), where sudden warming is followed by sudden cooling.

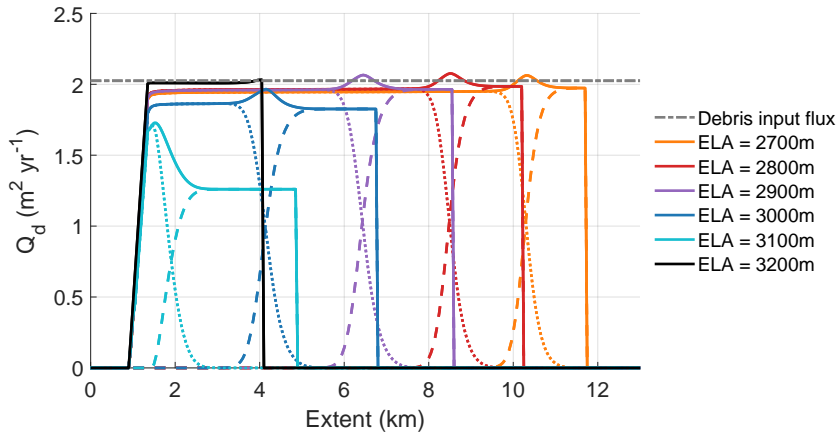


Figure B5. Along-glacier debris flux Q_d for 6 different ELA steady-states (2700–3200 m a.s.l.) given a constant d_{in} of 4.5 mm yr^{-1} . The total debris flux Q_d (solid lines) consists of the sum of the englacial (dotted lines) and the supraglacial (dashed lines) fluxes. The gray dash-dotted line represents the debris input flux $Q_{d,in} = d_{in} L_d$.

C1 Sensitivity to rate factor A

The rate factor A is a constant in Glen's flow law (Eq. 2) describing ice creep and dominantly depends on ice temperatures. Following the power law function with temperature (Cuffey and Paterson, 2010), temperate glaciers ($T = 0^\circ\text{C}$), should have a value of A of $2.4 \text{ s}^{-1} \text{ Pa}^{-3}$. For lower temperatures, A decreases significantly (e.g. $0.93 \text{ s}^{-1} \text{ Pa}^{-3}$ for -5°C). Data on ice temperatures in debris-covered glaciers is scarce. A recent study from Khumbu glacier shows polythermal conditions (Miles et al., 2018), with temperatures ranging from 0 to -3°C . In temperate climates with substantial surface melt in the accumulation area, such as the Alps, temperate ice conditions are prevailing (Suter et al., 2001). The rate factor can also be enhanced due to impurities within the ice (Cuffey and Paterson, 2010), but this effect is secondary and less well-constrained.

Similar as for clean-ice glaciers, for the initial steady state (ELA of 2900 m), we find a clear impact from a variable A on the glacier geometry (length and volume). A higher A leads to more ice deformation, which causes faster ice flow for the same thickness and ultimately results in a thinner and hence shorter glacier (Fig. C1). After a step-increase in ELA, we find that the transient response (relative length and volume change) is only weakly sensitive to the rate factor. Response times decrease only slightly for a high ($2.4 \text{ s}^{-1} \text{ Pa}^{-3}$) value of A , because the enhanced velocities from an increase in A accelerates geometric adjustment. We conclude that the transient response remains qualitatively similar irrespective of the choice in the rate factor, while quantitatively glacier geometry itself (and thus volume) is sensitive to A .

C2 Constraining of and sensitivity to the characteristic debris thickness D_0

The characteristic debris thickness D_0 describes how much insulation a given debris thickness can provide, or in other words, how fast the Østrem curve descends (the lower D_0 , the more insulation, the less melt). Therefore, changing D_0 by several cm

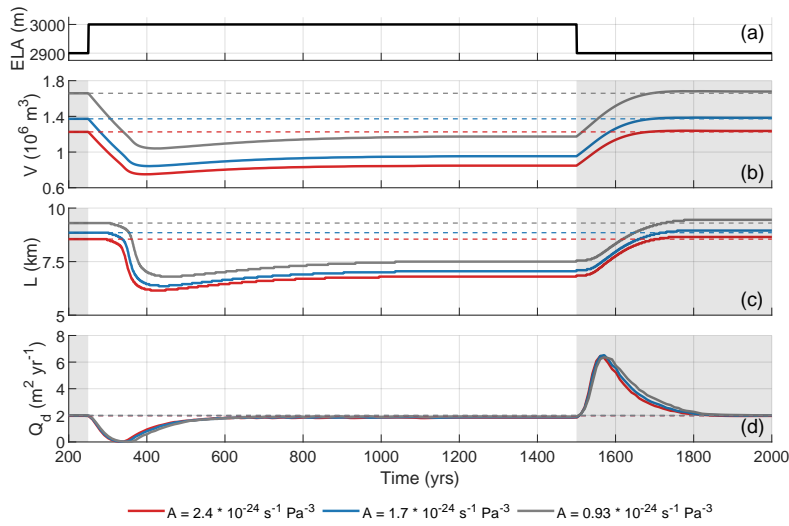


Figure C1. Transient sensitivity of the model for variable rate factors A when applying a step-change ELA forcing (a). (b) volume response, (c) length response, and (d) debris flux Q_d response 100 m up-glacier from the terminus.

745 leads to substantially different initial steady-state geometries (see initial length and volume in Fig. C3). Debris thickness and ablation data from real glaciers (Fig. C2a) show a wide spread and large differences between individual glaciers (Hardmeier, 2022). Consequently, estimates of D_0 can also vary substantially. Here, we examine the sensitivity of model results to values ranging between 0.05 m and 0.15 m, as shown in Figure C2b. Qualitatively, the transient response is somewhat affected by changes in D_0 (Fig. C3). Following the warming period, a low D_0 value (stronger insulation) results in a prolonged stagnant thinning phase (later retreat), a more abrupt but delayed retreat phase, and a longer, more pronounced rebounding effect. 750 This emphasizes the need for an accurate estimate of D_0 for modelling the evolution of a particular glacier. For the advance case, after a step-lowering of the ELA, the increase in ice flux and velocities combined with the already elongated tongue from a lower D_0 , gives rise to a more pronounced temporary debris flux surplus (Fig. C3d). However, this has no substantial consequence on the advance response (Fig. C3b & c). In general, the choice of D_0 does not affect the main conclusions made 755 in this study.

Author contributions. FH and AV designed the study. JCF and FH wrote the model code, FH conducted the numerical experiments. FH analyzed the synthetic data with support from JCF and AV. FH wrote the manuscript, AV and JCF edited and provided feedback during revisions.

Competing interests. The authors declare that they have no conflict of interest

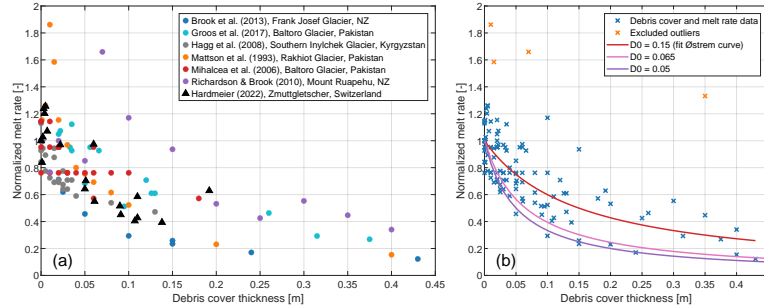


Figure C2. Relationship between debris cover thickness and melt rates normalized to clean ice (Østrem curve; adapted from Hardmeier (2022)). (a) Collated data points on normalized melt rates from literature (Brook et al., 2013; Groos et al., 2017; Hagg et al., 2008; Mattson et al., 1993; Mihalcea et al., 2006; Richardson and Brook, 2010; Hardmeier, 2022) coloured by publication and (b) Østrem curves according to Equation 10 using a D_0 of 0.05m (Ferguson and Vieli, 2021), 0.065m (Anderson and Anderson, 2016), and 0.15m used in this study from best fit to data shown in (a).

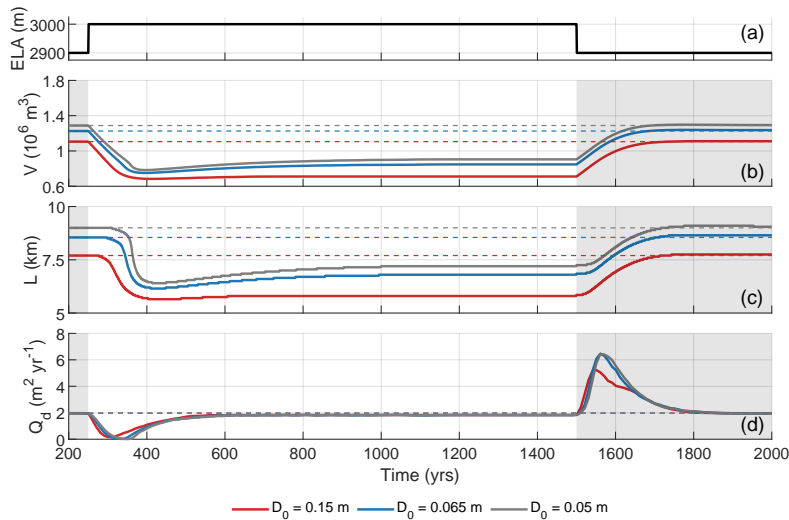


Figure C3. Transient sensitivity of the model for variable characteristic debris thickness D_0 when applying a step-change ELA forcing (a). (b) volume response, (c) length response, and (d) debris flux Q_d response 100m up-glacier from the terminus.

Acknowledgements. We thank Evan Miles, Ramachandran Shankar, and Argha Banerjee for valuable discussions and inputs on experiment design and analysis.



Financial support. This research has been mainly funded by the SNSF Grant IZINZ2_209521 within the Indo-Swiss joint trilateral SNSF-ICSSR-MoES scheme and the earlier SNSF Grant 200021_169775.



765 **References**

Anderson, L. S. and Anderson, R. S.: Modeling debris-covered glaciers: Response to steady debris deposition, *Cryosphere*, 10, 1105–1124, <https://doi.org/10.5194/TC-10-1105-2016>, 2016.

Anderson, L. S. and Anderson, R. S.: Debris thickness patterns on debris-covered glaciers, *Geomorphology*, 311, 1–12, <https://doi.org/10.1016/J.GEOMORPH.2018.03.014>, 2018.

770 Anderson, L. S., Armstrong, W. H., Anderson, R. S., Scherler, D., and Petersen, E.: The Causes of Debris-Covered Glacier Thinning: Evidence for the Importance of Ice Dynamics From Kennicott Glacier, Alaska, *Frontiers in Earth Science*, 9, 680995, [https://doi.org/10.3389/FEART.2021.680995/BIBTEX](https://doi.org/10.3389/FEART.2021.680995), 2021.

Anderson, R. S.: A model of ablation-dominated medial moraines and the generation of debris-mantled glacier snouts, *Journal of Glaciology*, 46, 459–469, <https://doi.org/10.3189/172756500781833025>, 2000.

775 Anderson, R. S., Anderson, L. S., Armstrong, W. H., Rossi, M. W., and Crump, S. E.: Glaciation of alpine valleys: The glacier – debris-covered glacier – rock glacier continuum, *Geomorphology*, 311, 127–142, <https://doi.org/10.1016/J.GEOMORPH.2018.03.015>, 2018.

Bahr, D. B., Pfeffer, W. T., Sassolas, C., and Meier, M. F.: Response time of glaciers as a function of size and mass balance: 1. Theory, *Journal of Geophysical Research: Solid Earth*, 103, 9777–9782, <https://doi.org/10.1029/98JB00507>, 1998.

Banerjee, A.: Brief communication: Thinning of debris-covered and debris-free glaciers in a warming climate, *Cryosphere*, 11, 133–138, <https://doi.org/10.5194/TC-11-133-2017>, 2017.

780 Banerjee, A. and Shankar, R.: On the response of Himalayan glaciers to climate change, *Journal of Glaciology*, 59, 480–490, <https://doi.org/10.3189/2013JOG12J130>, 2013.

Banerjee, A. and Wani, B. A.: Exponentially decreasing erosion rates protect the high-elevation crests of the Himalaya, *Earth and Planetary Science Letters*, 497, 22–28, <https://doi.org/10.1016/J.EPSL.2018.06.001>, 2018.

785 Bartlett, O. T., Ng, F. S., and Rowan, A. V.: Morphology and evolution of supraglacial hummocks on debris-covered Himalayan glaciers, *Earth Surface Processes and Landforms*, 46, 525–539, <https://doi.org/10.1002/ESP.5043>, 2021.

Benn, D. I. and Lehmkuhl, F.: Mass balance and equilibrium-line altitudes of glaciers in high-mountain environments, *Quaternary International*, 65–66, 15–29, [https://doi.org/10.1016/S1040-6182\(99\)00034-8](https://doi.org/10.1016/S1040-6182(99)00034-8), 2000.

Benn, D. I., Bolch, T., Hands, K., Gulley, J., Luckman, A., Nicholson, L. I., Quincey, D., Thompson, S., Toumi, R., and Wiseman, S.: <https://doi.org/10.1016/J.EARSCIREV.2012.03.008>, 2012.

790 Carturan, L., Filippi, R., Seppi, R., Gabrielli, P., Notarnicola, C., Bertoldi, L., Paul, F., Rastner, P., Cazorzi, F., Dinali, R., and Dalla Fontana, G.: Area and volume loss of the glaciers in the Ortles-Cevedale group (Eastern Italian Alps): Controls and imbalance of the remaining glaciers, *Cryosphere*, 7, 1339–1359, <https://doi.org/10.5194/TC-7-1339-2013>, 2013.

Compagno, L., Huss, M., Miles, E. S., McCarthy, M. J., Zekollari, H., Dehecq, A., Pellicciotti, F., and Farinotti, D.: Modelling supraglacial debris-cover evolution from the single-glacier to the regional scale: an application to High Mountain Asia, *Cryosphere*, 16, 1697–1718, <https://doi.org/10.5194/TC-16-1697-2022>, 2022.

800 Courant, R., Friedrichs, K., and Lewy, H.: Über die partiellen Differenzengleichungen der mathematischen Physik, *Mathematische Annalen*, 100, 32–74, <https://doi.org/10.1007/BF01448839>, 1928.



Cuffey, K. M. and Paterson, W. S. B.: The Physics of Glaciers, Elsevier, 4 edn., 2010.

Egholm, D. L., Knudsen, M. F., Clark, C. D., and Lesemann, J. E.: Modeling the flow of glaciers in steep terrains: The integrated second-order shallow ice approximation (iSOSIA), Volume 116, Issue 2, 116, <https://doi.org/10.1029/2010JF001900>, 2011.

805 Ferguson, J. C.: Modelling the dynamics and evolution of debris-covered glaciers, Ferguson, James Christopher. Modelling the dynamics and evolution of debris-covered glaciers. 2022, University of Zurich, Faculty of Science., <https://doi.org/10.5167/UZH-228173>, 2022.

Ferguson, J. C. and Vieli, A.: Modelling steady states and the transient response of debris-covered glaciers, *Cryosphere*, 15, 3377–3399, <https://doi.org/10.5194/TC-15-3377-2021>, 2021.

810 Fontrodona-Bach, A., Groeneveld, L., Miles, E., McCarthy, M., Shaw, T., Velasco, V. M., and Pellicciotti, F.: DebDaB: a database of supraglacial debris thickness and physical properties, *Earth System Science Data*, 17, 4213–4234, <https://doi.org/10.5194/ESSD-17-4213-2025>, 2025.

Fowler, A. C. and Larson, D. A.: On the flow of polythermal glaciers - I. Model and preliminary analysis, *Proceedings of the Royal Society of London. A. Mathematical and Physical Sciences*, 363, 217–242, <https://doi.org/10.1098/RSPA.1978.0165>, 1978.

815 Goosse, H., Barriat, P. Y., Dalaïden, Q., Klein, F., Marzeion, B., Maussion, F., Pelucchi, P., and Vlug, A.: Testing the consistency between changes in simulated climate and Alpine glacier length over the past millennium, *Climate of the Past*, 14, 1119–1133, <https://doi.org/10.5194/CP-14-1119-2018>, 2018.

Groos, A. R., Mayer, C., Smiraglia, C., Diolaiuti, G., and Lambrecht, A.: A First Attempt to Model Region-Wide Glacier Surface Mass Balances in the Karakoram: Findings and Future Challenges, *Geogr. Fis. e Dinam. Quat.*, 40, 137–159, <https://doi.org/10.4461/GFDQ.2017.40.10>, 2017.

820 Hagg, W., Mayer, C., Lambrecht, A., and Helm, A.: Sub-debris melt rates on southern inylchek glacier, central tian shan, *Geografiska Annaler: Series A, Physical Geography*, 90 A, 55–63, <https://doi.org/10.1111/J.1468-0459.2008.00333.X>, 2008.

Hardmeier, F.: Modelling climate sensitivity of debris-covered glaciers, Ph.D. thesis, University of Zurich, Zurich, 2022.

Hartmeyer, I., Delleske, R., Keuschnig, M., Krautblatter, M., Lang, A., Christoph Otto, J., and Schrott, L.: Current glacier recession causes significant rockfall increase: The immediate paraglacial response of deglaciating cirque walls, *Earth Surface Dynamics*, 8, 729–751, <https://doi.org/10.5194/ESURF-8-729-2020>, 2020.

825 Heimsath, A. M. and McGlynn, R.: Quantifying periglacial erosion in the Nepal high Himalaya, *Geomorphology*, 97, 5–23, <https://doi.org/10.1016/J.GEOMORPH.2007.02.046>, 2008.

Herreid, S. and Pellicciotti, F.: The state of rock debris covering Earth's glaciers, *Nature Geoscience* 2020 13:9, 13, 621–627, <https://doi.org/10.1038/s41561-020-0615-0>, 2020.

830 Johannesson, T., Raymond, C., and Waddington, E.: Time-Scale for Adjustment of Glaciers to Changes in Mass Balance, *Journal of Glaciology*, 35, 355–369, <https://doi.org/10.3189/S002214300000928X>, 1989.

Kirkbride, M. P. and Deline, P.: The formation of supraglacial debris covers by primary dispersal from transverse englacial debris bands, *Earth Surface Processes and Landforms*, 38, 1779–1792, <https://doi.org/10.1002/ESP.3416>, 2013.

Kneib, M., Fyffe, C. L., Miles, E. S., Lindemann, S., Shaw, T. E., Buri, P., McCarthy, M., Ouvry, B., Vieli, A., Sato, Y., Kraaijenbrink, P. D., Zhao, C., Molnar, P., and Pellicciotti, F.: Controls on Ice Cliff Distribution and Characteristics on Debris-Covered Glaciers, *Geophysical Research Letters*, 50, e2022GL102444, <https://doi.org/10.1029/2022GL102444>, 2023.

Langhammer, L., Rabenstein, L., Schmid, L., Bauder, A., Grab, M., Schaer, P., and Maurer, H.: Glacier bed surveying with helicopter-borne dual-polarization ground-penetrating radar, *Journal of Glaciology*, 65, 123–135, <https://doi.org/10.1017/JOG.2018.99>, 2019.



Lüthi, M. P.: Little Ice Age climate reconstruction from ensemble reanalysis of Alpine glacier fluctuations, *Cryosphere*, 8, 639–650, 840 <https://doi.org/10.5194/TC-8-639-2014>, 2014.

Margirier, A., Brondex, J., Rowan, A. V., Schmidt, C., Pedersen, V. K., Lehmann, B., Anderson, L. S., Veness, R., Watson, C. S., Swift, D., and King, G. E.: Tracking Sediment Transport Through Miage Glacier, Italy, Using a Lagrangian Approach With Luminescence Rock Surface Burial Dating of Englacial Clasts, *Journal of Geophysical Research: Earth Surface*, 130, e2024JF00773, <https://doi.org/10.1029/2024JF00773>, 2025.

845 Masson-Delmotte, V., Zhai, P., Chen, Y., Goldfarb, L., Gomis, M. I., Matthews, J. B. R., Berger, S., Huang, M., Yelekçi, O., Yu, R., Zhou, B., Lonnoy, E., Maycock, T. K., Waterfield, T., Leitzell, K., and Caud, N.: IPCC, 2021: Summary for Policymakers, *Climate Change 2021: The Physical Science Basis. Contribution of Working Group I to the Sixth Assessment Report of the Intergovernmental Panel on Climate Change*, www.ipcc.ch, 2021.

Mattson, L. E., Gardner, J. S., and Young, G. J.: Ablation on Debris Covered Glaciers: an Example from the Rakhiot Glacier, Punjab, 850 Himalaya, *Snow and Glacier Hydrology (Proceedings of the Kathmandu Symposium, November 1992)*, pp. 289–296, 1993.

Mayer, C. and Licciulli, C.: The Concept of Steady State, Cyclicity and Debris Unloading of Debris-Covered Glaciers, *Frontiers in Earth Science*, 9, 710 276, <https://doi.org/10.3389/FEART.2021.710276>, 2021.

McCarthy, M., Miles, E., Kneib, M., Buri, P., Fugger, S., and Pellicciotti, F.: Supraglacial debris thickness and supply rate in High-Mountain Asia, *Communications Earth & Environment* 2022 3:1, 3, 1–11, <https://doi.org/10.1038/s43247-022-00588-2>, 2022.

855 Mihalcea, C., Mayer, C., Diolaiuti, G., Lambrecht, A., Smiraglia, C., and Tartari, G.: Ice ablation and meteorological conditions on the debris-covered area of Baltoro glacier, Karakoram, Pakistan, *Annals of Glaciology*, 43, 292–300, <https://doi.org/10.3189/172756406781812104>, 2006.

Miles, K. E., Hubbard, B., Quincey, D. J., Miles, E. S., Sherpa, T. C., Rowan, A. V., and Doyle, S. H.: Polythermal structure of a Himalayan debris-covered glacier revealed by borehole thermometry, *Scientific Reports* 2018 8:1, 8, 1–9, <https://doi.org/10.1038/s41598-018-34327-5>, 2018.

860 Mölg, N., Bolch, T., Walter, A., and Vieli, A.: Unravelling the evolution of Zmuttgletscher and its debris cover since the end of the Little Ice Age, *Cryosphere*, 13, 1889–1909, <https://doi.org/10.5194/tc-13-1889-2019>, 2019.

Mölg, N., Ferguson, J., Bolch, T., and Vieli, A.: On the influence of debris cover on glacier morphology: How high-relief structures evolve from smooth surfaces, *Geomorphology*, 357, 107 092, <https://doi.org/10.1016/J.GEOMORPH.2020.107092>, 2020.

865 Moore, P. L.: Stability of supraglacial debris, *Earth Surface Processes and Landforms*, 43, 285–297, <https://doi.org/10.1002/ESP.4244>, 2018.

Nainwal, H., Banerjee, A., Shankar, R., Semwal, P., and Sharma, T.: Shrinkage of Satopanth and Bhagirath Kharak Glaciers, India, from 1936 to 2013, *Annals of Glaciology*, 57, 131–139, <https://doi.org/10.3189/2016AOG71A015>, 2016.

Nakawo, M., Yabuki, H., and Sakai, A.: Characteristics of Khumbu Glacier, Nepal Himalaya: recent change in the debris-covered area, *Annals of Glaciology*, 28, 118–122, <https://doi.org/10.3189/172756499781821788>, 1999.

870 Nicholson, L. and Benn, D. I.: Calculating ice melt beneath a debris layer using meteorological data, *Journal of Glaciology*, 52, 463–470, <https://doi.org/10.3189/172756506781828584>, 2006.

Oerlemans, J.: Estimating response times of Vadret da Morteratsch, Vadret da Palü, Brikdsalsbreen and Nigardsbreen from their length records, *Journal of Glaciology*, 53, 357–362, <https://doi.org/10.3189/002214307783258387>, 2007.

Østrem, G.: Ice Melting under a Thin Layer of Moraine, and the Existence of Ice Cores in Moraine Ridges, *Geografiska Annaler*, 41, 875 228–230, <https://doi.org/10.1080/20014422.1959.11907953>, 1959.



Pellicciotti, F., Stephan, C., Miles, E., Herreid, S., Immerzeel, W. W., and Bolch, T.: Mass-balance changes of the debris-covered glaciers in the Langtang Himal, Nepal, from 1974 to 1999, *Journal of Glaciology*, 61, 373–386, <https://doi.org/10.3189/2015JOG13J237>, 2015.

Ragettli, S., Bolch, T., and Pellicciotti, F.: Heterogeneous glacier thinning patterns over the last 40 years in Langtang Himal, Nepal, *Cryosphere*, 10, 2075–2097, <https://doi.org/10.5194/TC-10-2075-2016>, 2016.

880 Richardson, J. M. and Brook, M. S.: Ablation of debris-covered ice: Some effects of the 25 September 2007 Mt Ruapehu eruption, *Journal of the Royal Society of New Zealand*, 40, 45–55, <https://doi.org/10.1080/03036758.2010.494714>, 2010.

Rippin, D. M., Sharp, M., Van Wychen, W., and Zubot, D.: ‘Detachment’ of icefield outlet glaciers: catastrophic thinning and retreat of the Columbia Glacier (Canada), *Earth Surface Processes and Landforms*, 45, 459–472, <https://doi.org/10.1002/ESP.4746>, 2020.

Rounce, D. R., King, O., McCarthy, M., Shean, D. E., and Salerno, F.: Quantifying Debris Thickness of Debris-Covered Glaciers in the 885 Everest Region of Nepal Through Inversion of a Subdebris Melt Model, *Journal of Geophysical Research: Earth Surface*, 123, 1094–1115, <https://doi.org/10.1029/2017JF004395>, 2018.

Rowan, A. V., Egholm, D. L., Quincey, D. J., and Glasser, N. F.: Modelling the feedbacks between mass balance, ice flow and debris transport to predict the response to climate change of debris-covered glaciers in the Himalaya, *Earth and Planetary Science Letters*, 430, 427–438, <https://doi.org/10.1016/J.EPSL.2015.09.004>, 2015.

890 Rowan, A. V., Egholm, D. L., Quincey, D. J., Hubbard, B., King, O., Miles, E. S., Miles, K. E., and Hornsey, J.: The Role of Differential Ablation and Dynamic Detachment in Driving Accelerating Mass Loss From a Debris-Covered Himalayan Glacier, *Journal of Geophysical Research: Earth Surface*, 126, e2020JF005 761, <https://doi.org/10.1029/2020JF005761>; WGROUP:STRING:PUBLICATION, 2021.

Salerno, F., Thakuri, S., Tartari, G., Nuimura, T., Sunako, S., Sakai, A., and Fujita, K.: Debris-covered glacier anomaly? Morphological factors controlling changes in the mass balance, surface area, terminus position, and snow line altitude of Himalayan glaciers, *Earth and 895 Planetary Science Letters*, 471, 19–31, <https://doi.org/10.1016/J.EPSL.2017.04.039>, 2017.

Scherler, D. and Egholm, D. L.: Production and Transport of Supraglacial Debris: Insights From Cosmogenic ^{10}Be and Numerical Modeling, Chhota Shigri Glacier, Indian Himalaya, *Journal of Geophysical Research: Earth Surface*, 125, e2020JF005 586, <https://doi.org/10.1029/2020JF005586>, 2020.

Smolarkiewicz, P. K.: A Simple Positive Definite Advection Scheme with Small Implicit Diffusion, *Monthly Weather Review*, 111, 479–486, 900 1983.

Stewart, R., Westoby, M., Dunning, S., Rowan, A. V., and Woodward, J.: Exploring short-term rockfall inventories in deglaciating catchments: From evidencing glacial history to modelling rockfall runout, *Earth Surface Processes and Landforms*, 50, e70217, <https://doi.org/10.1002/ESP.70217>, 2025.

Suter, S., Laternser, M., Haeberli, W., Frauenfelder, R., and Hoelzle, M.: Cold firn and ice of high-altitude glaciers in the Alps: measurements 905 and distribution modelling, *Journal of Glaciology*, 47, 85–96, <https://doi.org/10.3189/172756501781832566>, 2001.

Thompson, S., Benn, D. I., Mertes, J., and Luckman, A.: Stagnation and mass loss on a Himalayan debris-covered glacier: processes, patterns and rates, *Journal of Glaciology*, 62, 467–485, <https://doi.org/10.1017/JOG.2016.37>, 2016.

Vacco, D. A.: Modeling glacier-rock-climate interactions: Moraine deposition, stagnation events, and supraglacial debris, Ph.D. thesis, Pennsylvania State University, <https://www.proquest.com/docview/304986423?pq-origsite=gscholar&fromopenview=true&sourcetype=Dissertations%20&%20Theses>, 2009.

910 Vacco, D. A., Alley, R. B., and Pollard, D.: Glacial advance and stagnation caused by rock avalanches, *Earth and Planetary Science Letters*, 294, 123–130, <https://doi.org/10.1016/J.EPSL.2010.03.019>, 2010.



van Woerkom, T., Steiner, J. F., Kraaijenbrink, P. D., Miles, E. S., and Immerzeel, W. W.: Sediment supply from lateral moraines to a debris-covered glacier in the Himalaya, *Earth Surface Dynamics*, 7, 411–427, <https://doi.org/10.5194/ESURF-7-411-2019>, 2019.

915 Verhaegen, Y., Huybrechts, P., Rybak, O., and Popovnin, V. V.: Modelling the evolution of Djankuat Glacier, North Caucasus, from 1752 until 2100CE, *Cryosphere*, 14, 4039–4061, <https://doi.org/10.5194/TC-14-4039-2020>, 2020.

Westoby, M. J., Rounce, D. R., Shaw, T. E., Fyffe, C. L., Moore, P. L., Stewart, R. L., and Brock, B. W.: Geomorphological evolution of a debris-covered glacier surface, *Earth Surface Processes and Landforms*, 45, 3431–3448, <https://doi.org/10.1002/ESP.4973>, 2020.

920 Wirbel, A., Jarosch, A. H., and Nicholson, L.: Modelling debris transport within glaciers by advection in a full-Stokes ice flow model, *Cryosphere*, 12, 189–204, <https://doi.org/10.5194/TC-12-189-2018>, 2018.

Zekollari, H. and Huybrechts, P.: On the climate–geometry imbalance, response time and volume–area scaling of an alpine glacier: insights from a 3-D flow model applied to Vadret da Morteratsch, Switzerland, *Annals of Glaciology*, 56, 51–62, <https://doi.org/10.3189/2015AOG70A921>, 2015.